R-01-48

Conductive fracture mapping

A study on the correlation between borehole TV- and radar images and difference flow logging results in borehole KLX02

Seje Carlsten, Allan Stråhle, Jan-Erik Ludvigson
GEOSIGMA AB

October 2001

Svensk Kärnbränslehantering AB
Swedish Nuclear Fuel
and Waste Management Co
Box 5864
SE-102 40 Stockholm Sweden
Tel 08-459 84 00
+46 8 459 84 00
Fax 08-661 57 19
+46 8 661 57 19

ISSN 1402-3091
SKB Rapport R-01-48

Conductive fracture mapping

A study on the correlation between borehole TV- and radar images and difference flow logging results in borehole KLX02

Seje Carlsten, Allan Stråhle, Jan-Erik Ludvigson
GEOSIGMA AB

October 2001

Keywords: Difference flow logging (DIFF), Borehole TV (BIPS), Borehole Radar

Abstract

This study presents an attempt to correlate images from borehole-TV (BIPS) and borehole radar with interpreted flow anomalies from Difference Flow Meter logging (DIFF). The measurements were performed in the interval 200–400 m in borehole KLX02 at Laxemar. In total, 59 flow anomalies were interpreted by the DIFF-log in this borehole interval. However, 14 flow anomalies were below the rigorous measurement limit for the actual flow meter and are thus regarded as uncertain.

In total, 261 features were primarily interpreted by the BIPS-characterization in the borehole interval 200–400 m but only 12 radar reflectors. The low number of interpreted radar reflectors most likely depends on the low frequency of the antenna used in this case which gave a poor depth resolution. The total number of fractures recorded by the core mapping in this interval was 374 (279 in the rock together with 95 fractures in interpreted crush zones).

Prior to the correlation analysis it was necessary to adjust the length scales of the BIPS-measurements relative to the length scale of the Difference Flow logging due to non-linear stretching of logging cables etc to achieve the necessary resolution of the depth scale. This adjustment was done by comparing the distances between clearly identified single features in the BIPS-images with the corresponding distances between clearly identified flow anomalies. The BIPS-measurements consist of 5 independent logging sequences in the studied borehole interval, which resulted in "jumps" when comparing the non-conform length scales of the different sequences.

All of the 59 flow anomalies could be correlated (matched) with BIPS-features with varying degree of certainty. A majority of the correlated BIPS-features was classified as open fractures or fractures with cavities. Most of the flow anomalies below the measurement limit were correlated to veins in the rock.

In the correlation between borehole radar reflectors and BIPS-features, the calculated α-angle and the recorded borehole length were used as the most important parameters. The accuracy of the recorded length (depth) of the interpreted radar reflectors is rather poor compared to the BIPS-logging. A total number of 6 radar reflectors (of the 12 identified) could be correlated with BIPS-features and DIFF-flow anomalies. As above, the correlated BIPS-features were classified as open fractures or in some cases as veins in the rock.

The correlation study indicates that the number of features mapped as "open fractures" together with "fractures with cavities" in the BIPS characterisation, correspond to almost 70% of the total number of interpreted flow anomalies from the DIFF-logging in this borehole interval. This figure increases to almost 80% if uncertain flow anomalies below the measurement limit are excluded. The remainder of the flow anomalies correspond to features mapped as "altered fractures or veins" and "dull fractures or veins" in the BIPS-characterisation.

The estimated lateral extent of the correlated radar reflectors is about 10–30 m. The latter figure corresponds to the estimated persistence (depth of penetration) of the radar images in this case.

The dominant strike of the interpreted flow anomalies is towards WNW-NW as determined from the BIPS-and radar characterisation. This result is in good agreement with previous investigations of the orientation of water-conductive fractures at Äspö. Thus, it is concluded that the interpreted flow anomalies from the DIFF-log are representative for the dominating hydraulic conditions in the rock.

The accuracy of the depth recording is one of the most important parameter and also the one that, in this study, contributes to the largest error when comparing different methods. One of the conclusions of this study is to diminish the error by using efficient measuring wheels in order to avoid sliding of the cable during logging. A new method for making length registration is at present under development. Also, certainty and conformity of the reference level of each individual method is crucial.

Provided that the adjustment of the length scales of the different logging methods does not bias the studied correlation between the logging methods, this study appear to yield promising results with regards to structural-hydrogeological interpretations and models. However, improved depth resolution of the radar measurements is required. Finally, correct length scales of the logging sequences, preferably by using reference depth marks in the boreholes, are crucial for the correlation.

Contents

Sammanfattning

Denna studie presenterar ett försök att korrelera bilder från borrhåls-TV (BIPS) och borrhålsradar med tolkade flödesanomalier från differensflödesloggning (DIFF). Mätningarna var utförda i intervallet 200–400 m i borrhål KLX02 på Laxemar. Totalt 59 flödesanomalier var tolkade från DIFF-loggningen i detta borrhålsintervall. 14 av dessa flödesanomalier var emellertid under den strikta mätgränsen för den aktuella flödesmätaren och får därför betraktas som osäkra.

Totalt tolkades 261 objekt från BIPS-karaktäriseringen i borrhålsintervallet 200–400 m men bara 12 radarreflektorer. Det låga antalet tolkade radarreflektorer beror sannolikt på den låga frekvensen på den antenn som användes i detta fall som gav en dålig djupupplösning. Det totala antalet sprickor från kärnkarteringen i detta intervall var 374 (279 i bergmassan och 95 sprickor i tolkade krosszoner).

Före korrelationen var det nödvändigt att justera längdskalorna i BIPS-mätningarna i förhållande till längdskalan för differensflödesloggningen på grund av icke-linjär töjning av loggingkablarna etc. för att uppnå den erforderliga upplösningen i längdskalan. Denna justering gjordes genom att jämföra avstånden mellan klart identifierade enstaka objekt i BIPS-bilderna med motsvarande avstånd mellan klart identifierade flödesanomalier. BIPS-mätningarna består av 5 oberoende loggningssekvenser i det studerade borrhålsintervallet, vilket resulterar i ”hopp” vid jämförelse av de icke-konforma längdskalorna för de olika sekvenserna.

Alla 59 tolkade flödesanomalier kunde korreleras (matchas) med BIPS-objekt med varierande grad av säkerhet. En majoritet av de korrelerade BIPS-objekten var klassificerade som öppna sprickor eller sprickor med kaviteter. De flesta av flödesanomalierna under mätgränsen korrelerades med bergartsgångar.

Vid korrelationen mellan borrhålsradarreflektorerna och BIPS-objekten användes de beräknade α-vinklarna och mätt borrhålslängd som de mest viktiga parametrarna. Noggrannheten av den mätta längden (djupet) av de tolkade radarreflektorerna är ganska dålig jämfört med BIPS-loggningen. Ett totalt antal av 6 radarreflektorer (av de 12 identifierade) kunde korreleras med BIPS-objekt och DIFF-flödesanomalier. Som ovan klassificerades de korrelerade BIPS-objekten som öppna sprickor eller i några fall som bergartsgångar.

Korrelationsstudien indikerar att antalet objekt som karterats som ”öppna sprickor” tillsammans med ”sprickor med kaviteter” i BIPS-karaktäriseringen, motsvarar nästan 70 % av det totala antalet tolkade flödesanomalier från DIFF-loggningen i detta borrhålsintervall. Denna siffra ökar till nästan 80 % om osäkra flödesanomalier under mätgränsen utesluts. Resterande flödesanomalier motsvarar objekt klassificerade som ”omvandlade sprickor eller gångar” och ”matta sprickor eller gångar” i BIPS-karaktäriseringen.

Den uppskattade laterala utbredningen av de korrelerade radarreflektorerna är cirka 10–30 m. Den senare siffran motsvarar den uppskattade genomträngningen (penetrationsdjup) i radargrammen i detta fall.

Den dominerande strykningen av de tolkade flödesanomalierna är mot VNV-NV bestämd från BIPS- och radarkaraktäriseringen. Detta resultat är i god överens-stämmelse med tidigare undersökningar av orienteringen på konduktiva sprickor på Äspö. Sålunda dras slutsatsen att de tolkade flödesanomalierna från DIFF-loggen är representativa för de dominerande hydrauliska förhållandena i berget.

Noggrannheten i djupmätningen är en av de mest viktiga parametrarna och också den som, i denna studie, bidrar till det största felet vid jämförelse av olika metoder. En av slutsatserna i denna studie är att minska felet genom att använda effektiva mäthjul för att undvika kabelglidning under loggning. En ny metod för att göra längdregistrering är för närvarande under utveckling. Även säkerhet och överensstämmelse av referensnivån för varje individuell metod är avgörande.

Förutsatt att justeringen av längdskalorna för de olika loggningsmetoderna inte påverkar den studerade korrelationen mellan loggningsmetoderna, verkar denna studie ge lovande resultat med avseende på struktur-hydrogeologiska tolkningar och modeller. Förbättrad djupupplösning för radarmätningarna krävs emellertid. Slutligen, korrekta längdskalor för loggningssekvenserna, helst genom användande av referensdjupmärken i borrhålen, är avgörande för korrelationen.

1 Introduction

As a co-operative work between SKB and Posiva, the Posiva Difference Flow meter Log was tested in KLX02 at Laxemar. The borehole interval 200–1400 m was measured. Two field campaigns were carried out, Campaign 1 in February–March 2000 and Campaign 2 in May–June 2000. The first campaign mainly involved sequential (normal mode) flow measurements in 3-m sections and fresh water head measurements along the hole.

During the second campaign, overlapping (detailed mode) flow logging was performed in 0.5-m sections, successively moved in 0.1-m steps. This logging was combined with measurements of the electric conductivity, both of the borehole fluid and in the fractures. /Rouhiainen 2000/ reported the results of the difference flow logging in KLX02 at Laxemar with the Posiva Flow Log during both Campaigns 1 and 2.

In conjunction with the second campaign, a special methodology study was performed in the borehole interval c. 200–400 m. The main purpose of this study was to test whether overlapping flow logging could also be used to determine the hydraulic transmissivity of the interpreted flowing fractures. In addition, some alternative measurement strategies were tested to provide a basis for the design of an "optimal" test program for difference flow logging for site investigations. The methodology study of the difference flow meter in KLX02 constitutes a separate project and is reported in /Ludvigson et al, 2001/.

Besides the methodology study, a correlation between the results of the present difference flow logging and the previous borehole-TV (BIPS)- and radar investigations in this borehole interval was also performed. The borehole-TV measurements in KLX02 are unpublished and only stored at the SKB-database SICADA whereas the radar investigations are reported in /Carlsten 1993/. The difference flow logging offers a unique possibility to separate and correlate individual, flowing fractures with the results of other measurements, provided that a common depth scale can be established between the different measurement methods.

The present study utilises results from the overlapping difference flow logging in the interval 200–400 m of borehole KLX02. The (position of) the interpreted flowing fractures in this borehole interval are used as the primary data set. These fractures are then correlated with the results of previous borehole-TV- and radar measurements. Top of casing was used as the common reference level by the correlation.

2 Objectives

The main purpose of this study is to correlate the interpreted flowing fractures from overlapping flow logging with the results of previous borehole TV (BIPS) – and radar investigations. The correlation firstly involves a depth correlation of the flowing fractures along the borehole between the different methods and subsequently a geological characterisation and geometrical interpretation of the fractures. In addition, major discrepancies between the methods are analysed and discussed, e.g. major BIPS- and/or radar anomalies not interpreted as flowing fractures by the flow logging.

The positions of flowing fractures are primarily deduced from the difference flow logging together with their estimated transmissivity and natural head. The geological characterisation (rock type, degree of fracturing etc.) is mainly made from the BIPS-images. The results of the core mapping in this borehole interval are difficult to adjust to a common length scale with the other methods and are therefore only used as supporting data in this study. From the BIPS-interpretation also the orientation (strike/dip) and a measure of the total aperture of the fractures together with the intersection angle (α) between the fracture and borehole. The information deduced from the BIPS-measurements represents near-borehole information.

The radar measurements may provide geometrical information of the fractures at a certain distance from the borehole. Thus, the orientation (strike/dip) and a rough estimation of the extension of the fractures as deduced from the radar images may be obtained. The degree of detail depends though strongly on the resolution (frequency) of the radar measurements.

The ultimate goal of this study is to test and develop a combined tool for a complete characterisation of flowing fractures regarding their position and geological, hydraulic and geometrical properties. Such information may be useful in e.g. discrete network modelling and other near-field modelling and for assessments of the hydraulic connectivity pattern in fractured rock.

3 Difference flow meter measurements

3.1 Principles of measurement

Posiva Flow Log using the Difference Flow Meter (DIFF) can be used for relatively fast determination of the position and hydraulic properties of flowing fractures or fractured zones. The changes of flow along the borehole are measured rather than the cumulative flow as for conventional flow meters. This increases the resolution of the method and its capability to identify individual flowing fractures. In addition, the direction of the flow in the fractures can be determined (into or out of the borehole). /Öhberg and Rouhiainen, 2000/ describe the method in detail.

The flow along the borehole outside the test section is directed through the flow guide, so that it does not pass the flow sensor, see Figure 3-1. Thus, the flow into or out from the test section is the only flow that passes through the flow sensor. Small flow (0.1–10 ml/min) and the corresponding flow direction is measured from the transit time and direction of a thermal pulse injected in the sensor. Measurements of high flow (2–5,000 ml/min) and direction is based on the thermal dilution rate of monitoring sensors.

Instead of inflatable packers, rubber disks are used at both ends of the flow guide to isolate the section to be measured. The rubber disks are designed in such a way that they are always pressed against the borehole wall. Thus, no additional hydraulic pressure differences are applied in the test section relative to the remaining part of the hole. The advantage of using rubber discs instead of inflatable packers is that moving the tool along the hole is fast and the low risk for the equipment to get stuck in the hole /Öhberg and Rouhiainen, 2000/.

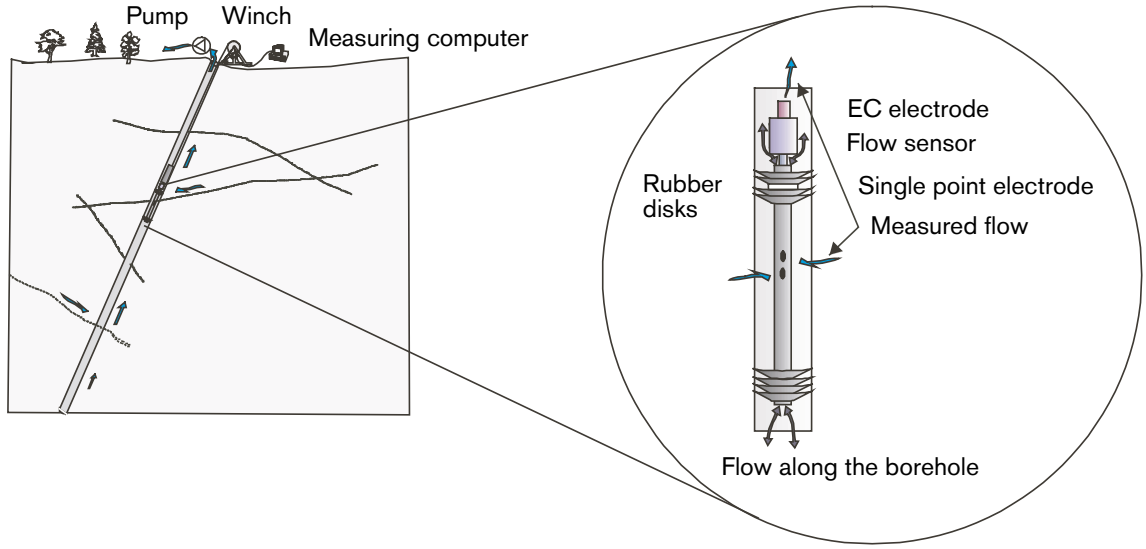

Figure 3-1. *Schematic picture of the downhole equipment used in the DIFF flow meter. From /Rouhiainen, 2000/.*

In surface boreholes, difference flow measurements can be performed during natural conditions without pumping the borehole and when the borehole is pumped at a constant drawdown. The hydraulic head along the borehole is then assumed to be constant since the hydraulic conductivity of the borehole is very high compared to the conductivity of the bedrock. Consequently, the difference in head across the rubber disks used to isolate the test section is very small.

Constant hydraulic head in the borehole implies that the water density in the hole is constant (both under natural conditions and during pumping) and that there are no losses due to friction. If this is not the case the hydraulic head at the measuring depth needs to be determined. Since the density of saline water is higher than density of fresh water, the fresh water head has to be measured in such cases. In cases of saline water, the term fresh water head is used instead of hydraulic head, since hydraulic head is not well defined in saline conditions /Rouhiainen, 2000/.

An option of the flow meter tool is the electrode to measure the electrical conductivity and temperature of the groundwater (EC) along the hole with a special measuring geometry. This may be a good indication of the possible rise of saline water during pumping. During overlapping flow logging it is possible to measure the electrical conductivity and temperature of specific groundwater from selected flowing fractures, simultaneously with the flow measurement, see Figure 3-1. This requires that the hole is pumped so that the flow is directed from the fractures into the borehole.

The single point resistance measurement is another option in the flow meter tool. The electrode of the single point resistance tool is located within the upper rubber disks, see Figure 3-1. This sensitive method is used for exact depth determination of flowing fractures and geological structures.

3.2 Performance

Difference flow meter measurements can be carried out in two different measurement modes (sequential and overlapping measurements, respectively) depending on the purpose and scale of measurement, see Table 3-1. Previously, the measurement modes were called normal and detail mode, respectively /Öhberg and Rouhiainen, 2000/. Sequential logging is mainly used to obtain the hydraulic conductivity and natural fresh water head of borehole sections, e.g. 3-m. Overlapping logging, which is carried out in shorter sections, is used for more precise depth determination of single flowing fractures or fracture zones along the hole. The overlapping logging can be extended to also determine the transmissivity of individual fractures /Rouhiainen, 2000/.

Table 3-1. Technical specifications of Posiva Difference flow meter. After /Öhberg and Rouhiainen, 2000/.

Mode	Type of Flow measurement	Flow range (ml/min)	Time of measurement	Scale of measurement
Sequential	– Thermal pulse – Thermal dilution	0.1–10 2–5,000	c. 15 min/test section	Borehole sections, e.g. L=3 m
Overlapping	Thermal dilution	2–5,000	c. 10 s/measurement	Flowing fractures, e.g. L=0.5–1 m, dL=0.1 m

Since the results (i.e. the position of flowing fractures) of the overlapping flow logging in KLX02 are used in this study, the description below is focussed on such logging. The overlapping logging is performed in short sections, e.g. 0.5 m or 1 m, which are moved stepwise in small increments, e.g. 0.1 m, along the hole under natural and/or pumped conditions. Furthermore, overlapping flow logging is performed only by the thermal dilution method to speed up the measurements, see Table 3-1. For determination of the depths to flowing fractures, only one flow logging sequence is required. If the hydraulic properties (transmissivity, head etc.) of the flowing fractures are to be determined, at least two logging sequences (at different drawdown in the hole) must be carried out / Rouhiainen 2000, Ludvigson et al, 2001/.

The duration of a flow measurement with the thermal dilution method is 10 s at each depth. This means that with a section length of 0.5–1.0 m and 0.1-m step length, about 10–15 m/h of borehole length can be measured during overlapping flow logging /Öhberg and Rouhiainen, 2000/, see Table 3-1. The overlapping measurements can be done automatically without the presence of an operator.

3.3 Results and data quality

The locations of the interpreted flowing fractures together with the corresponding flow rates at different drawdowns in the hole, as interpreted by /Rouhiainen, 2000/ are presented in Appendix 1. The overlapping logging was performed in the borehole interval 200–400 m, starting at c. 204 m and stopping at c. 406 m. All depths are given with "top of casing" as reference level. A long line represents the depth of a ("certain") flowing fracture whereas a short line indicates that the existence of the fracture is uncertain.The measurement range for overlapping logging is from 2 ml/min (120 ml/h) to 5,000 ml/min (300,000 ml/h), see Table 3-1. Measured flows below 2 ml/min (120 ml/h) are uncertain. Furthermore, the measured single point resistance log and the previous caliper log are presented in Appendix 1.

During the overlapping logging in the interval 200–400 m in KLX02, only very small effects of rising saline water in the borehole were noticed, as inferred from the EC-loggings of the borehole water before and after the measurements /Rouhiainen, 2000/. Thus, the density was assumed to be constant along the hole in this borehole interval and no effects of changing density need to be considered in this case.

The interpreted positions and flow rates of the interpreted flowing fractures from the DIFF-log at 22-m drawdown together with their calculated transmissivities are presented in Table 3-2. In some of the fractures, zero flow was measured at 22-m drawdown although small flows (below the measurement limit) were measured at smaller drawdowns. Such interpreted flow anomalies, which are considered as uncertain, are within brackets in Table 3-2. On the other hand, one additional potential flowing fracture at a depth of c.385.4 m is included in the table. The noise level changed significantly at this depth, see below.

In the present study, mainly the interpreted positions and flows of the interpreted flowing fractures in the measured borehole interval are utilised. The quality of the data from the flow logging is regarded as good. The results are consistent regarding the interpreted positions of the fractures between the measurement sequences with different drawdowns.

The vertical length of the plotted flow anomalies in Appendix 1 corresponds to the section length minus the step length used, i.e. in this case 0.4 m, even if the flow comes from a single fracture. By convention, the flowing fracture is always located at the lower limit of the anomaly in the plots /Rouhiainen, 2000/. If the distance between flowing fractures is less than 0.4 m the anomalies will be overlapped in this case. Flowing fractures near each other can better be resolved with a short section- and step length.

On the other hand, measurements with a short section length can be misleading where the borehole wall is in "bad" condition (e.g. due to cavities) longer than the section length, see e.g. the depths of c. 219 m and c. 385 m. No flowing fractures were interpreted at these depths. However, the results are uncertain due to long cavities along the hole, which may cause leakage during the flow logging. According to the core mapping results in /Stanfors et al, 1997, p 81/, the rock is tectonized at 219 m with increased fracture frequency. At c. 385 m, a crush zone associated with a greenstone vein occurs with a significant increase of fracture frequency. In Table 3-2 a potential flowing fracture at 385.4 m has been included.

Table 3-2. Interpreted depth, flow rate and transmissivity of flowing fractures at 22 m drawdown together with depths of major noise of the baseflow. Uncertain flowing fractures are within brackets. From /Ludvigson et al, 2001/.

Depth (m)	Q (s=22m) (ml/h)	T (m^2/s)	Noise (ml/h)	Depth (m)	Q (s=22m) (ml/h)	T (m^2/s)	Noise (ml/h)
212.0	2964	3.6×10^{-8}		268.0	16905	2.1×10^{-7}	
213.3	158662	1.9×10^{-6}		269.0	213	2.5×10^{-9}	
214.0	16757	2.0×10^{-7}		269.7	7977	9.7×10^{-8}	
215.2	5031	6.1×10^{-8}		271.1	36168	4.4×10^{-7}	
216.7	302	3.6×10^{-9}		273.8	715	8.5×10^{-9}	
220.7	572	6.8×10^{-9}		(275.0	0	–)	
224.4	12542	1.5×10^{-7}		276.9	462	5.5×10^{-9}	
224.9	1823	2.2×10^{-8}		290.5	796	9.5×10^{-9}	
226.0	6625	7.9×10^{-8}		292.6	219	2.6×10^{-9}	
227.7	30680	3.7×10^{-7}		295.1	30324	3.6×10^{-7}	
231.9	778	9.2×10^{-9}		295.6	4393	5.2×10^{-8}	
232.4	38	–		298.3	698	8.3×10^{-9}	
233.9	5337	6.4×10^{-8}		300.6	801	9.5×10^{-9}	
234.2	166	2.0×10^{-9}		(307.9	0	–)	
237.8	359	4.3×10^{-9}		(310.5	0	–)	
238.0	86	–		(314.7	0	–)	
239.1	604	7.2×10^{-9}		317.1	452519	5.5×10^{-6}	100➥300
241.4	990	1.2×10^{-8}		(325.4	0	–)	
242.3	121	–		(327.8	0	–)	
243.3	2870	3.5×10^{-8}		(328.6	0	–)	
243.8	714	8.5×10^{-9}		(329.2	0	–)	
244.9	733	8.7×10^{-9}		(332.7	0	–)	
246.7	22150	2.7×10^{-7}		337.9	9576	1.2×10^{7}	
248.6	15479	1.9×10^{-7}		338.9	12983	1.7×10^{-7}	
249.2	1623	2.0×10^{-8}		339.1	34185	4.2×10^{-7}	300➥500
250.1	578	6.9×10^{-9}		339.6	717	1.0×10^{-8}	
251.3	458764	5.5×10^{-6}	20➥100	(377.2	0	–)	
251.6	111455	1.4×10^{-6}		(383.5	0	–)	
252.9	41867	5.0×10^{-7}		385.4*	c. 15000	–	500➥20
254.1	1269	1.6×10^{-8}		389.3	375	4.5×10^{-9}	

* potential flowing fracture not interpreted by Rouhiainen (2000).

A “noise” in the baseflow rate was observed in the overlapping logging with 22-m drawdown, especially during the combined flow rate/EC measurements at certain flow anomalies, see Table 3-2. Most depths, at which the noise level changed significantly, correspond to flowing fractures with rather high inflow rate and transmissivity. In addition, large single point resistance anomalies occur at these depths, see Appendix 1.

One possible reason for the noise at 22 m drawdown is gas in the water from some fractures /Rouhiainen, 2000/. All the measurements were carried out from the surface downward. At 22-m drawdown, more gas might enter into the test section because of the higher pumping rate and because the tool was stopped on some fractures for the fracture-specific EC-measurements. The gas could possibly escape from the section when the upper rubber disks arrived to the widened part of the borehole at the large caliper anomalies. This might explain the decrease in the noise level at c. 385-m. Other possible reasons to the noise are discussed in /Ludvigson et al, 2001/.

4 Borehole television measurements

4.1 Performance and data quality

The borehole-TV system used was the BIPS (**B**orehole **I**mage **P**rocessing **S**ystem) from RaaX Co., Ltd. BIPS uses a conical mirror to create a planar image that covers the walls 360º. An image-processing unit produces a rolled out image that covers all 360°. The recorded image covers 360º from left to right and is continuous along the borehole. North or the high side is in the middle of the image. In vertical (85–90º) boreholes an electronic compass is used. The image recording takes place, as the probe is slowly (1.5 m/min) lowered down the borehole. The processed image file is recorded on MO disks, with about 1 MB/m.

BIPS TV-images from KLX02 were created during 1994–2000. The quality of the images varies considerably. The best images are the oldest, due to a black substance on the borehole wall, which has precipitated through time. The images used were amongst the earliest, logged on April 19–20, 1994, see Table 4-1. Later produced logs were poorer in quality.

The BIPS-images are logged with standard resolution, which means 1.0 mm along the borehole and 0.66 mm (∅=76 mm) around the borehole wall. The quality of the images used is in general considered as good.

The fact that the BIPS-logging was performed in a non-successive order, and not on the same day, means that the depth correlation between the sections is not linear and therefore not very easy to perform. Consequently, there will appear "jumps" in the correction factors of the depth scales in the correlation log.

A regular fracture mapping of the BIPS images log was performed firstly. The mapping included orientation and characterisation of each individual fracture. Also observed veins were mapped. The characterisation was done by using the standard SKB BIPS characteristics chart. In the mapping, open fractures and fractures with cavities (partly open) were considered as potentially water conductive. A table showing all interpreted structures from the BIPS-images is presented in Appendix 2.

Table 4-1. List of the BIPS-images used in different borehole sections.

Section	Logging date	Logging time
203–245 m	940419	15:22
245–290 m	940419	16:01
290–340 m	940420	11:16
340–390 m	940420	11:57
390–440 m	940419	12:32

4.2 Correlation strategy between BIPS and flow logging

The correlation between the interpreted flowing fractures from the flow logging and fractures mapped in the BIPS images was performed by firstly correlating clearly open fractures from the latter images with large flow anomalies. A list of the depths of the correlated fractures was then produced. The list consists of two depth values for each anomaly, one depth value from the flow log and one from the BIPS-recorded length. This list revealed the order of the differences of the two length scales, so it was possible to roughly adjust the length scales of the interpreted flowing fractures and the BIPS image length scale.

The correlation list shows "jumps" of the correction factors when shifting from one BIPS file to the next. These "jumps" are the results from not logging in one sequence, which fact decreases the accuracy of the correction in those parts.

By using the inter-flow spot distances and inter-fracture distances it was possible to establish a flow spot pattern to be compared with the BIPS-recorded fracture pattern. To check if the correct flow point/fracture pairs were found, the difference between the two sub-distances was calculated. A certain variation of this difference is natural as it is dependent on where the main flow is located along the fracture. The BIPS-mapping refers to the point where the fracture plane cuts the centre line of the hole or the core but the depth of the flow spot refers to the actual point where the flow occurs. If the difference of the sub-distance was less than 30 cm between the methods, the correlation was considered as good. Larger differences were regarded as an uncertain correlation.

In summary, the correlation of the interpreted flow spots and the BIPS-images was performed in three steps:

1. Firstly, an overall length correlation was performed, based on the major flow spots and BIPS-features.
2. Secondly, all correlated flow spots were classified according to the BIPS- characterisation of these. Features characterised as open and cavities, respectively under "condition", were regarded as most probable for correlation with the flow spots. Features characterised as dull or apparent flow spots associated with mapped veins were regarded as less probable.
3. Finally, a comparison between the inter-fracture distances and the inter-flow spot distances was used as a classification tool. Large differences of these distances indicated less probability of finding the right feature.

4.3 Results of correlation between BIPS and flow logging

The correlation between the interpreted flow spots and open and partly open fractures (cavities) from the BIPS-characterisation was good, although a small number of flow spots were mapped as "dull" fractures, e.g. fractures with fracture minerals and/or fracture surface alteration. There was also a few flow spots which were impossible to correlate with the BIPS-images due to absence of trace in the BIPS image within a reasonable distance from calculated position of the flow spot. The reasons for this can be bad length correlation, very thin low-conductive fracture or imperfect position of the flow meter regarding cavities etc in the borehole. Which one and how these factors may affect the correlation has not been investigated.

As discussed above, some of the 59 interpreted flow spots exhibited small flows which were below the rigorous measurement limit for flow (2 ml/min) and are thus uncertain. Such fractures may exhibit a poor correlation with open , or partly open BIPS-features. A table with the results of the final correlation between the interpreted flow anomalies and the BIPS mapping is presented in Appendix 3. Flow anomalies below the measurement limit are marked with a “B” and uncertain flow anomalies with a “U”. The judged certainty of the correlation is also indicated in the table. BIPS images showing all the correlated flow anomalies can be seen in Appendix 4 (red figures correspond to adjusted depths).

4.4 Uncertainties

At about 385 m, the flow loggings indicated a high flow value, but no flow anomaly is determined here. The caliper log indicates large cavities between 383.5–389.3 m, with a maximum at 385.3 m. The BIPS image confirms that this is a highly fractured zone with considerable rock fall-out. As discussed in the previous section, the results of the flow logging may be uncertain due to possible leakage at the rubber discs within the cavity. Thus, the potential flow anomaly at 385.0 m in Appendix 3 is uncertain.

5 Borehole radar measurements

5.1 Performance and data quality

A radar probe with a transmitter and a receiver is lowered into the borehole. The transmitter generates an electromagnetic pulse, which propagates through the rock surrounding the borehole. Fractures, fracture zones, crushed zones, lithological contacts, etc. constitutes structures in the rock mass having diverging electrical properties compared to the rock mass. The difference in electrical property makes the structures work as reflectors for the radar pulses. Reflected pulses are recorded by the receiver and stored in a field computer. The principles for a radar measurement are shown in Figure 5-1.

The radar probe is lowered into the borehole and measurement is performed stepwise. For the measurement in KLX02 a steps of 0.5 m was used. The steps are dependent on the frequency of the probe, which in this case was a 60 MHz directional antenna. The directional antenna consists of an array of four loop antennas, which makes it possible to synthesise the direction of the incoming radar pulse.

The radar measurement in KLX02 was performed during three runs in July 7 and 8, 1993. The interruption during July 8 was caused by exchange of batteries in the probe. The borehole was measured between 209.55–1034.55 m. The quality of the radar

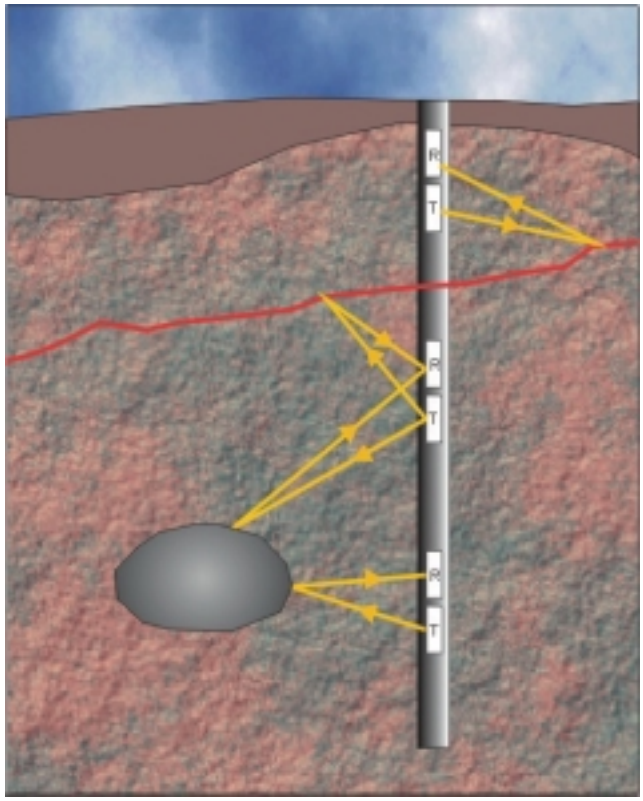

Figure 5-1. *Principles for a radar measurement. Transmitter (T) and receiver (R) are located in the same borehole.*

measurement in the section between 209–400 m is considered good. The penetration of radar waves in a radius around the borehole is about 25–30 m. A radar map with interpreted reflectors is found in Appendix 5.

The accuracy in intersection length of radar reflectors with borehole is dependent on (i) the frequency of the radar pulse (ii) the angle between borehole axis and reflector (iii) the tension of the cable (iv) and the accuracy of the measuring wheel over which the cable runs. The accuracy depending on the frequency and the intersection angle is ±2 m in this particular measurement. However, for reflectors having small intersection angle to the borehole axis, the accuracy may be less. The measuring wheel probably contributes to the largest error in the accuracy of the intersection length. This error is due to slip and slide of the cable during start, movement, and stop between each measure point.

5.2 Correlation strategy between radar and BIPS

Correlation between borehole radar and BIPS borehole-TV has previously been made in boreholes at the Äspö HRL and in boreholes in the Boda area. Äspö HRL is located at the eastern coast of Sweden 330 km south of Stockholm and Boda is located at the eastern coast of Sweden 320 km north of Stockholm /Carlsten and Stråhle, 2000/. The results from the correlations were successful.

The interpretation of the intersection with borehole of radar structures has a much larger inaccuracy compared to the interpretation of intersection of BIPS-structures. Therefore, the intersection length of the radar reflectors has been given a lower priority in the correlation process. The angle between structure and borehole axis (alpha angle) for both radar reflectors and BIPS-structures is one of the most important parameters in the correlation process and has therefore been given highest priority. Next parameter in the correlation process is the agreement between radar orientation and BIPS-orientation. The third parameter is the intersection length, mentioned above.

The correlation of each radar reflector with a BIPS-structure was performed in the following manner. The intersection length from the radar interpretation works as an indicator of where to start the search for suitable structures in the BIPS pictures. The search of structures in the BIPS pictures was limited to ±5m from the interpreted radar intersection, i.e. due to the larger uncertainty of radar intersection. Adjusted lengths in the BIPS pictures have been used for the correlation. The alpha angle between radar reflector and BIPS-structure was then compared. If the difference was considered acceptable then the radar orientation and the BIPS-orientation was compared. It should be noted that the orientation of a radar reflector is based on reflections from a structure outside the borehole and over a quite large distance, while the orientation from BIPS is based on a very small area inside the borehole.

A discussion about the difference between radar measurement performed with the directional antenna (KLX02) and the newly produced dipole antenna probes is held in Chapter 7. With the radar frequency used in this case, single fractures can only be detected in favourable cases. In general, more large-scale features, such as fracture zones, rock veins and rock contacts can be seen.

5.3 Results of correlation between radar and BIPS

The results presented in this chapter are primarily based on the correlation between radar and BIPS. The subsequent correlation between the radar measurements and the interpreted flow anomalies is based on the results from the correlation between BIPS and flow anomalis, described in the previous Chapter, due to the low depth resolution of the actual radar measurements.

Nevertheless, the results of the correlation between radar and BIPS are considered satisfying, regarding the fact that directional antenna measurements may only detect rather large and persistent structures, while the BIPS- and flow measurements can identify single and narrow fractures on a scale of centimetres.

A total number of 12 radar reflectors have been interpreted to intersect within the borehole interval 200–400 m. A radar interpretation map is shown in Appendix 5. A table with the results from the correlation between radar and BIPS is presented in Appendix 6. Of the 12 identified radar reflectors, 10 could be correlated with BIPS structures. The agreement between the alpha angles from radar and BIPS is considered good. The agreement between the interpreted orientations of the structures is also considered good. The only exception is the orientation of reflector 4-1, which is 352/73 (strike/dip) in the radar measurements compared to the orientation of 119/77 for the corresponding BIPS-structure. However, there is larger discrepancy when comparing the intersection lengths between radar reflectors and BIPS structures. Explanations to this are given in Chapter 5.2.

The lower limb of radar reflector 4-1 at 212 m can be observed to a distance of 30 m outside the borehole. The agreement between alpha angles for radar and BIPS is very good, and the difference in depth is very small. However, the radar orientation (352/73) and the BIPS orientation (119/77) differ somewhat. BIPS shows a fracture at 212.1 m. The flow measurement shows an anomaly at 212.0 m and a larger anomaly at 213.3 m. The BIPS log also shows an open fracture at 213.7 m which is parallel to the fracture at 212.1 m. It is possible that the radar reflector might indicate both fractures.

The upper limb of radar reflector 5-2 can be observed to a distance of 20 m outside the borehole. The agreement between alpha angles is good, but the depth correlation differs several meters (BIPS at 246.6 m and radar at 251 m). The radar orientation (175/53) and the BIPS orientation (136/45) agree rather well. BIPS shows an open fracture at 246.6 m. The flow measurement shows increased values at 246.7 m.

The medium strong radar reflector 6-2 at 262 m is sub-parallel to reflector 5-2. The upper limb can be observed to a distance of 18 m outside the borehole. The agreement between alpha angles for radar and BIPS is relatively good and the intersection length is also considered good. The radar orientation 292/49 and the BIPS orientation 321/32 agree well with each other. BIPS mapping shows oxidised fracture at 260.3 m. However, the flow log indicates no change at this depth.

Radar reflector 7-3 is strong and occurs at 269 m. The upper limb can be observed to a distance of about 22 m outside the borehole. The agreement between alpha angle for radar and BIPS is good as well as the agreement between intersection length. Also, the agreement between orientation is considered good. BIPS mapping shows open fracture at 267.8 m. The flow log shows increased value at 268.0 m.

Lower limb of the strong reflector 8-3 intersects the borehole at 271 m. The reflector can be observed to a distance of about 30 m outside the borehole. The agreement between radar angle and BIPS angle is very good and the agreement in intersection length is also good. The radar orientation and the BIPS orientation also agree well. There is an open fracture at 269.5 m according to BIPS mapping. The flow log shows increased values at 269.7 m.

Radar reflector 9-1 at 280 m has a weak character in the radar map. The reflector can be traced to a distance of 20 m outside the borehole. However, there is no suitable BIPS structure at this depth and the flow log shows no increased values at this depth.

The medium strong radar reflector 10-2 at borehole length 296 m can be observed to a distance of 17 m outside the borehole. There are not any suitable BIPS structures at this depth, and thereby there has not been possibility to correlate the radar structure with the flow log.

Radar reflector 11-3 at 341 m is strong and both upper and lower limb of the reflector can be seen in the radar map. The upper limb can be traced to a distance of 31 m and the lower limb to 22 m outside the borehole, i.e. the structure has an observed extension of more than 50 m. The alpha angle of the corresponding BIPS structure is 54° and the radar angle is 59°. Radar orientation is 270/24 and BIPS orientation is 241/35. BIPS mapping shows open fracture at 338.8 m. The flow log shows increased value at 339.1 m. The correlation is considered good.

Reflector 12-1 at 367 m is weak and can be traced to a distance of 18 m outside the borehole. The correlation between alpha angles is good as well as between the orientations. BIPS mapping shows the presence of a chlorite vein at 363.9 m. However, the flow log does not show increased value at this depth.

The upper limb of reflector 13-2 at 388 m can be observed to a distance of 35 m outside the borehole. The lower limb of the reflector is probably one of the several parallel reflectors interpreted as reflector 14-2 and 15-1. The alpha angle 61° for the reflector agrees very well with the BIPS alpha angle 64° at 385.0 m length. However, the BIPS structure represents a fracture having a different orientation than the majority of open fractures within the fractured greenstone section between 280–400 m in the borehole. A renewed interpretation based on the newly additional BIPS mapping is presented in the chapter below. The radar orientation 012/30 and the BIPS orientation 020/28 agrees very well.

Lower limb of reflector 14-2 at 394 m consists in the radar map of a couple of parallel reflectors. The reflector can be traced to a distance of about 15 m outside the borehole. The alpha angle of radar reflector and the BIPS structure at 391.5 m show good agreement. Also, the orientation for the radar reflector (047/38) and the BIPS structure (054/49) show good agreement. There is no flow log available at this depth.

Reflector 15-1 at 396 m has a weak character in the radar map. The reflector can be traced to a distance of 15 m outside the borehole. The alpha angle of the radar reflector is 44° and corresponds well to the BIPS alpha angle which is 53° for a structure at 396.1 m. The agreement for the radar orientation, which is 045/51 and the BIPS orientation, which is 031/40, is good. There is no flow log available at this depth.

5.4 Uncertainties and reinterpretation

The section between 380–400 m contains several parallel reflectors. A majority of the reflectors are rather strong and also parallel to each other. The alpha angle is mainly steep i.e. 50–70°. Reflectors 13, 14, and 15 probably indicate a section with pegmatite and greenstone. However, the BIPS mapping shows the presence of several open fractures within this section. The radar amplitude exhibits a distinct section with low values between 384–385 m. Decreased amplitude values is normally caused by higher fracture frequency (higher porosity) or by a different rock type (different electrical properties). The flow log indicated an increased flow at c. 385 m.

The interpretation in the radar report /Carlsten, 1993/ indicated that the amplitude change in this section was caused by a fractured greenstone. The detailed BIPS mapping, on the other hand, show that the greenstone and the open fractures have different directions. A renewed control of the radar map shows that there is a radar reflector (N2-1), obscured by the several parallel reflectors, which might represent the open fractures. The radar reflector is best observed in the azimuth maps used for the interpretation, but in the radar map can the upper limb of the reflector be seen close to the borehole. The lower limb is only observed in the azimuth maps and not in the dipole map presented in this report. Thus, there are two possible orientations for reflector N2-1. This is due to difficulties in the interpretation caused by the interference with the steeply, parallel reflectors. The orientation alternatives are 166/62 or 353/60. Best fit is achieved with the radar orientation 353/60 compared to BIPS orientation 355/65 at borehole length 384.66 m. The alpha angle from BIPS is 25° and the alpha angle from radar is 29°.

6 Combined correlation

The combined correlation of the results from the flow logging, borehole television (BIPS) and borehole radar is presented in Appendix 7. The table shows firstly the depths of the interpreted flow spots from the flow logging and the adjusted depths and orientations of correlated features from the BIPS-mapping. In addition, the mapped sort (fracture, vein etc.) and width of these features in the borehole are shown together with their conditions (cavities, open, dull etc.) and BIPS-correlation class (certain, medium and uncertain). From the borehole radar correlation, the associated radar depth, orientation, persistence and radar class of the correlated flow spots are shown.

The table in Appendix 7 shows that it was possible to correlate all interpreted 59 flow anomalies with BIPS-features with a varying degree of certainty (BIPS-class). The correlation of the majority of the flow anomalies were classified as "certain" by the BIPS-correlation. The table also indicates that the most high-conductive fractures generally correspond to fractures mapped as "open" or "cavities" in the BIPS-characterisation. Several of the uncertain flow spots below the measurement limit correspond to "veins" in the BIPS-characterisation. The uncertain fracture at c. 385 m in Table 3-2 from the flow logging corresponds to an open fracture.

The correlation with the radar measurements shows that only 6 of the 12 interpreted radar anomalies can be correlated with flow anomalies. As discussed above, this is due to the lower resolution of the radar measurements for the frequency used. However, some of the flow anomalies are clustered within a spacing of a few centimetres or decimetres between each flow anomaly. Fractures with such a high density are not possible to separate when using a long wavelength of the radar pulse as with the directional antenna in this case.

Plots showing the estimated orientation of the 59 flow anomalies from the BIPS- correlation are shown in Figure 6-1 and Figure 6-2. Two main groups of fractures can be identified, the first striking towards WNW and relatively steeply dipping towards NE. The second group is striking towards NW and rather steeply dipping towards SW. A third group is striking towards NE and dipping towards SE. However, the third group consists of only a few structures, and some of them are representing veins or a lithological contact. These results are in good agreement with previous investigations of the orientations of water-conductive features at Äspö /Mazurek et al, 1996/.

Figure 6-3 shows the distribution of the cumulative "aperture" (width) from the BIPS-characterisation of the interpreted flow anomalies along the investigated borehole interval. It should be observed that this "aperture" is not the hydraulic fracture aperture but rather the mapped width of the BIPS-feature in the borehole.

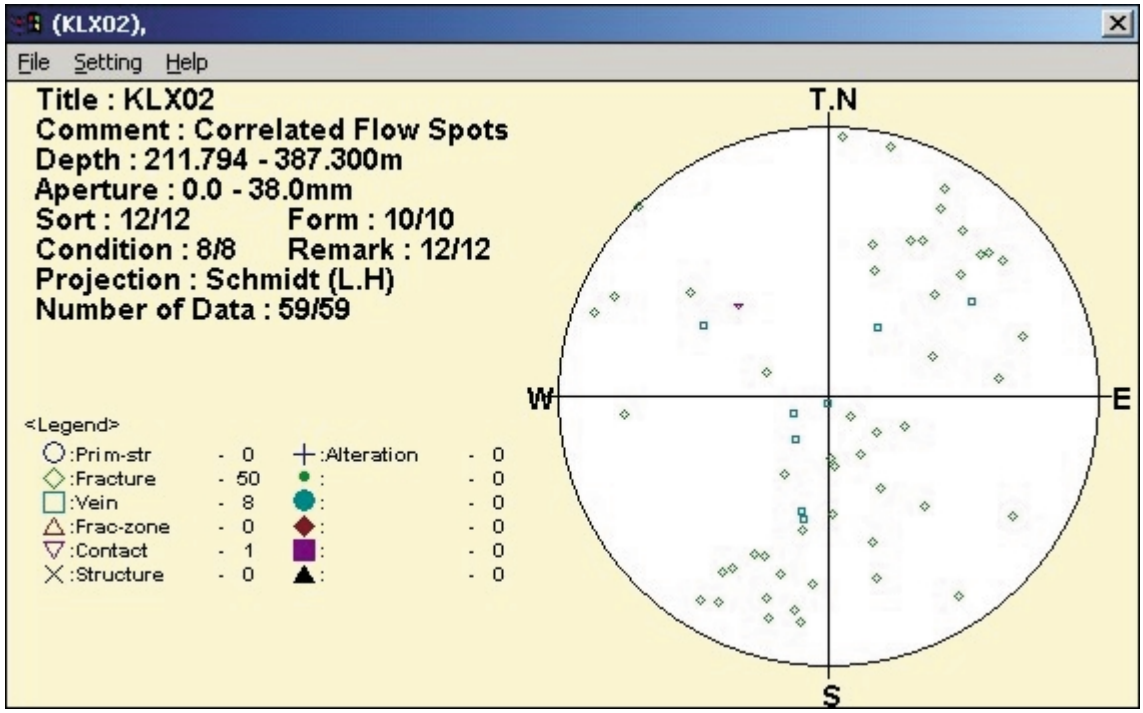

Figure 6-1. *Stereogram showing normals to structures mapped by borehole television and correlated with flow spots in the interval 200–400 m in KLX02.*

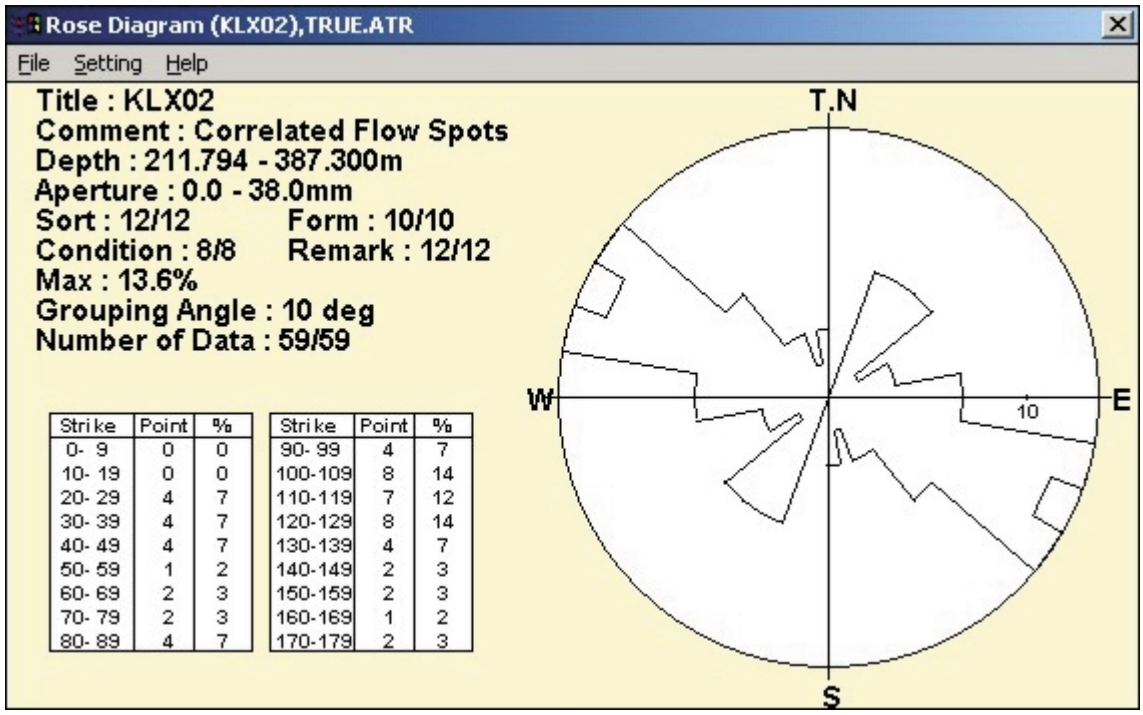

Strike	Point	%
0- 9	0	0
10- 19	0	0
20- 29	4	7
30- 39	4	7
40- 49	4	7
50- 59	1	2
60- 69	2	3
70- 79	2	3
80- 89	4	7

Strike	Point	%
90- 99	4	7
100-109	8	14
110-119	7	12
120-129	8	14
130-139	4	7
140-149	2	3
150-159	2	3
160-169	1	2
170-179	2	3

Figure 6-2. *Rose diagram with direction of structures mapped by borehole television and correlated with flow spots in the interval 200–400 m in KLX02.*

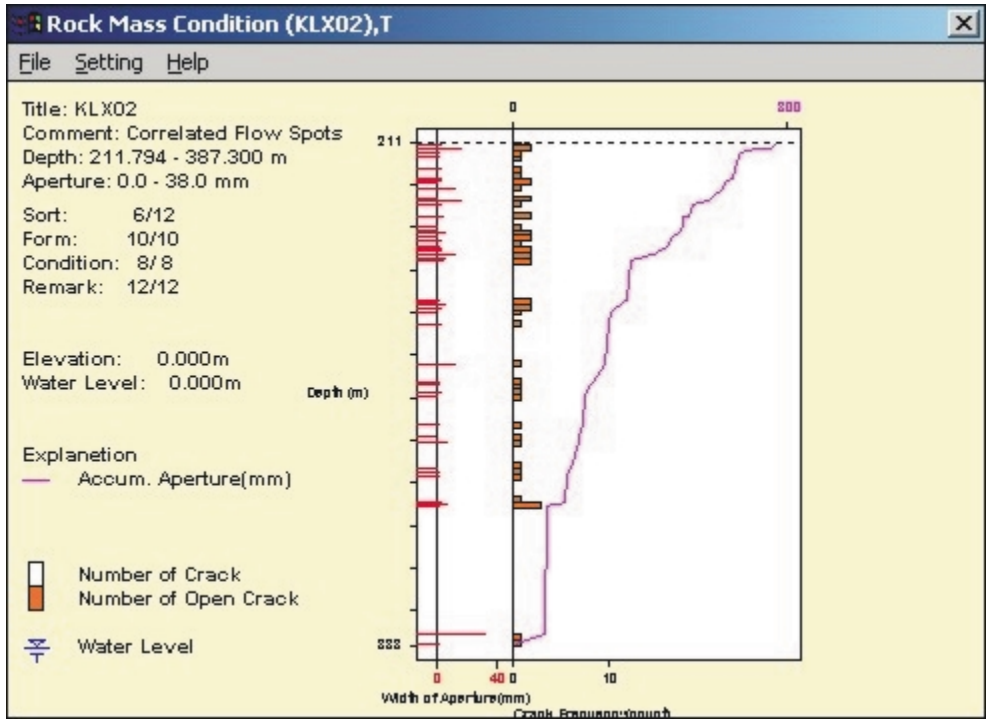

Figure 6-3. *Diagram showing (from left): 1) aperture (width), 2) fracture frequency, 3) accumulated aperture (width) of BIPS-features within the interval of 200–400 m in borehole KLX02.*

In Table 6-1, the BIPS-characterisation of the correlated flow anomalies in the borehole interval 200–400 m is shown. The table firstly shows the total number of BIPS-characterised features according to Appendix 2, divided in different classification groups. Secondly, the number of flow anomalies (shown in Table 3-2) which could be correlated with these BIPS-features in each group are shown. As discussed above, it was possible to correlate all the 59 interpreted flow anomalies with BIPS-features. Some of the flow anomalies were though below the actual measurement limit (120 ml/h) and thus uncertain. In total, 45 of the interpreted 59 flow anomalies exhibited a flow above the measurement limit, c.f. Table 3-2. The distribution of these 45 flow anomalies in the different BIPS-groups is also shown in Table 6-1 (within brackets). In addition, the associated percentages of correlated flow anomalies of all the BIPS-features in each group are shown.

Table 6-1. Number of BIPS-characterised features in different groups and correlated flow anomalies to BIPS-features in these groups. Interval 200–400 m in KLX02.

Groups of BIPS-characterised features	Number of BIPS-features	Number of correlated flow anomalies to BIPS-features		Percentage of correlated flow anomalies to BIPS-features	
Open fractures	19	16	(16)	84	(84)
Fractures with cavities	39	24	(19)	62	(49)
Altered fractures or veins	89	6	(2)	7	(2)
Dull fractures or veins	114	13	(8)	11	(7)
Total, all groups	261	59	(45)	23	(17)

For example, of the 19 BIPS-features mapped as “open fractures”, 16 (84%) could be correlated with one of the interpreted flow anomalies in Table 3-2 and correspondingly, 24 (62%) of the 39 BIPS-features mapped as “fractures with cavities”. On the other hand, of features mapped as “altered fractures or veins”, only c. 7% could be correlated with flow anomalies. On average, c. 23% of all BIPS-features (261) could be correlated with the flowing fractures. For comparison, the total number of fractures in the rock, recorded from the core mapping, in this borehole interval was 279 plus 95 fractures in interpreted crush zones, i.e. totally 374 fractures /Ludvigson et al, 2001/.

It may be expected that most of the interpreted flow anomalies would correspond to open fractures or fractures with cavities and that fractures characterised as dull or oxidised would be less represented. Table 6-1 shows that this is also the case, although there are some features that do not fit into this pattern. The total number of interpreted flow anomalies within the first two groups (40) correspond to almost 70% of all the interpreted flow anomalies (59). If uncertain flow anomalies are excluded, this figure increases to almost 80% (35/45) since most of the uncertain flow anomalies fall into the last two groups in Table 6-1 (oxidised and dull fractures or veins). The number of correlated, “certain” flow anomalies correspond to figures within brackets in the table.

Possible reasons for the deviations from this pattern are:

- Poor control of the length scale of the measurements due to the fact that the old BIPS-logging was performed in several sequences.
- Small inter-fracture distances. Closely spaced flow spots may interact with each other.
- Instrumental and/or measurement deficiencies. Both the results of the BIPS as well as the flow measurements and the performance of the instruments may be uncertain in some cases, e.g. in damaged borehole intervals with cavities.

7 Conclusions and recommendations

This study showed that it was possible to correlate all 59 flow anomalies, interpreted from the difference flow logging, with BIPS-features with varying degree of certainty. The majority of the correlation of the flow anomalies are classified as "certain" by the BIPS-correlation. Most of the flowing fractures (c. 70–80%) correspond to fractures mapped as "open" and "fractures with cavities" in the BIPS-characterisation. This is regarded as a significant result.

Of the BIPS-features mapped as "open fractures", 84% could be correlated with the interpreted flow anomalies in this group and 62% of features mapped as "fractures with cavities". On the other hand, of features mapped as "altered fractures or veins", only c. 7% could be correlated with flow anomalies. The total number of interpreted features from the BIPS-mapping was 261. On average, c. 23% of all BIPS-features could be correlated to flowing fractures. From the core mapping, the total number of fractures in this borehole interval was 374 (279 in the rock and 95 in crush zones).

The results of the correlation between borehole radar and BIPS was considered successful. However, only 12 radar reflectors were identified between 200–400 m. Of these, 10 reflectors could be correlated with corresponding structures from the BIPS mapping. Two of them was not possible to correlate neither with BIPS nor with flow anomalies. The agreement between the 10 correlated reflectors and the BIPS-mapping was good, except for one where the difference in alpha angle is 21°, and another one where the difference in orientation is large.

Six of the reflectors could be correlated both with BIPS and with flow anomalies. The fact that the radar is represented by such a few number of reflectors is dependent on the rather low antenna frequency (60 MHz) used in these particular measurements. With the radar frequency used in this case, single fractures can only be detected in favourable cases. In general, more large-scale features, such as fracture zones, rock veins and rock contacts can be seen.

The radar measurements in KLX02 were performed in 1993 using a radar equipment which is no longer in use. The frequency of the used directional antenna was 60 MHz. A much better resolution of radar measurements is achieved when using the newly developed 100 MHz and 250 MHz dipole antennas. Measurements performed at the Äspö HRL and in the Boda area using 100 MHz and 250 MHz antennas have shown that even single fractures can be detected by the radar and correlated with BIPS structures /Carlsten and Stråhle, 2000/. However, the dipole antennas give no information about the strike of the structures, only intersection length with borehole and the alpha angle is given. The orientation of structures can be obtained from the BIPS measurement.

The advantage of combining the radar and BIPS methods is that the borehole radar gives evidence of the continuation and persistence of structures outside the borehole, while BIPS gives information on the character of the structures in the borehole and the orientation of the identified structure.

The accuracy of the intersection length of radar reflectors is dependent on the used frequency of the antenna, the alpha angle, the tension of the cable, and the accuracy of the measuring wheel. The largest contribution of error is probably received from the measuring wheel. The error is not linear since it consists of small slip and slides of the cable during movements up or down during measurement. A different type of measuring wheel, which diminishes these types of errors, is now in use. Also, measurements with the dipole antenna is performed continuously and without any stops. This helps to prevent errors caused by slip and slide of the cable.

When comparing BIPS, radar and flow anomalies it has to be kept in mind that the different logging methods have been performed with a gap of several years. This fact implies that the pre-conditions, e.g. requirements on precision and resolution of the measurements, may have changed. This might contribute to inaccuracies between the three methods.

To overcome the problems with length scale adjustment, it will be most rewarding to concentrate on the length correlation of each of the different methods used. This work would have been much easier, quicker and with better quality, if the methods were performed in a way, that made a direct correlation possible. Fortunately, a new method for making length markers in the borehole is under development.

The problem with small inter-fracture distances is harder to overcome, as the flow logging measures in a fixed section, although it is small, fractures that sometimes interact with each other.

Instrument error and non-representative measurements may always be a problem. BIPS resolution, for example, can be increased from 1 mm to 0.25 mm. This would, at least theoretically, be an improvement in finding the fractures. In intervals where the borehole wall is in bad condition, e.g. due to cavities, the results of the Difference Flow log may be uncertain due to the risk of untight rubber discs, particularly with short section lengths.

To conclude, with the combined correlation of the results from Difference Flow logging, BIPS- and radar measurements it was possible to identify and localise the flowing fractures along the hole, determine their orientation and estimate their extension. The inferred orientation of the interpreted flow anomalies is in good agreement with previous studies of the orientation of water-conductive features at Äspö. The estimated extension of the flow anomalies ranges from c. 10–30 m according to the radar measurements. The persistence (depth of penetration) of the latter measurements is c. 30 m from the borehole.

References

Carlsten S, 1993. Drilling KLX02 – Phase 2 Lilla Laxemar, Oskarshamn – Borehole radar measurements in KLX02.
SKB AR 93-43, Svensk Kärnbränslehantering AB

Carlsten S, Stråhle A, 2000. Borehole radar and BIPS investigations in boreholes at the Boda area.
SKB TR-01-02, Svensk Kärnbränslehantering AB

Ludvigson J-E, Hansson K, Rouhiainen P, 2001. Methodology study of Posiva Difference Flow Meter in borehole KLX02 at Laxemar.
SKB R-01-52 (in prep), Svensk Kärnbränslehantering AB

Mazurek M, Bossart P, Eliasson T, 1996. Classification and characterization of water-conducting features at Äspö: Results of investigations on the outcrop scale.
International Cooperation Report 97-01, Svensk Kärnbränslehantering AB

Rouhiainen P, 2000. Difference flow measurements in borehole KLX02 at Laxemar. Äspö Hard Rock Laboratory.
SKB IPR-01-06, Svensk Kärnbränslehantering AB

Stanfors R, Erlström M, Markström I, 1997. ÄSPÖ HRL – Geoscientific evaluation 1997/1. Overview of site characterization 1986–1995.
SKB TR-97-02, Svensk Kärnbränslehantering AB

Öhberg A, Rouhiainen P, 2000. Posiva groundwater flow measuring techniques.
Report Posiva 2000-12

Appendix 1

Difference flow meter log in the interval 200–400 m in KLX02

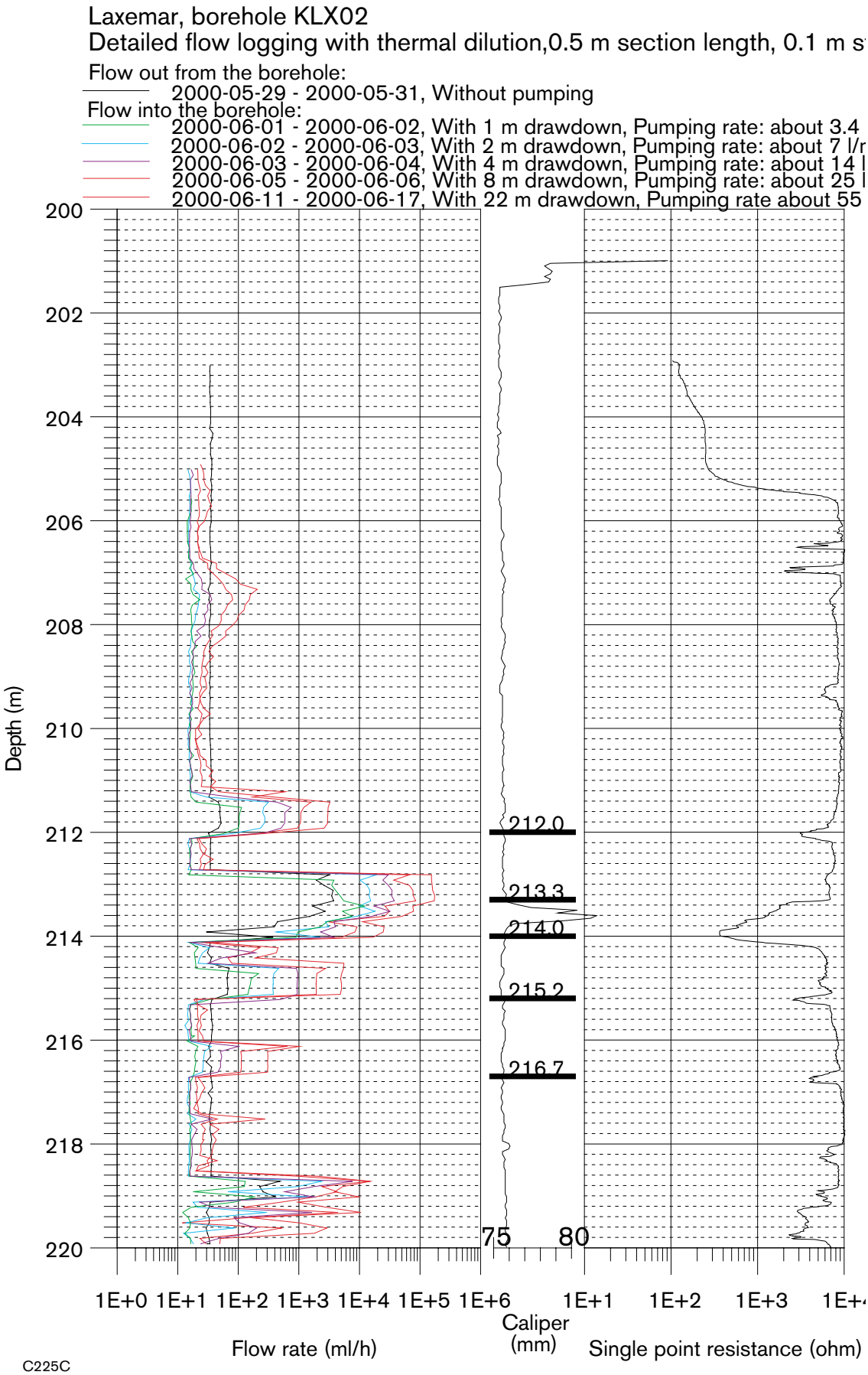
Laxemar, borehole KLX02
Detailed flow logging with thermal dilution,0.5 m section length, 0.1 m s
Flow out from the borehole:
2000-05-29 - 2000-05-31, Without pumping
Flow into the borehole:
2000-06-01 - 2000-06-02, With 1 m drawdown, Pumping rate: about 3.4
2000-06-02 - 2000-06-03, With 2 m drawdown, Pumping rate: about 7 l/r
2000-06-03 - 2000-06-04, With 4 m drawdown, Pumping rate: about 14 l
2000-06-05 - 2000-06-06, With 8 m drawdown, Pumping rate: about 25 l
2000-06-11 - 2000-06-17, With 22 m drawdown, Pumping rate about 55
Depth (m)
200
202
204
206
208
210
212
214
216
218
220
212.0
213.3
214.0
215.2
216.7
75
80
1E+0 1E+1 1E+2 1E+3 1E+4 1E+5 1E+6
1E+1 1E+2 1E+3 1E+4
Flow rate (ml/h)
Caliper (mm)
Single point resistance (ohm)
C225C

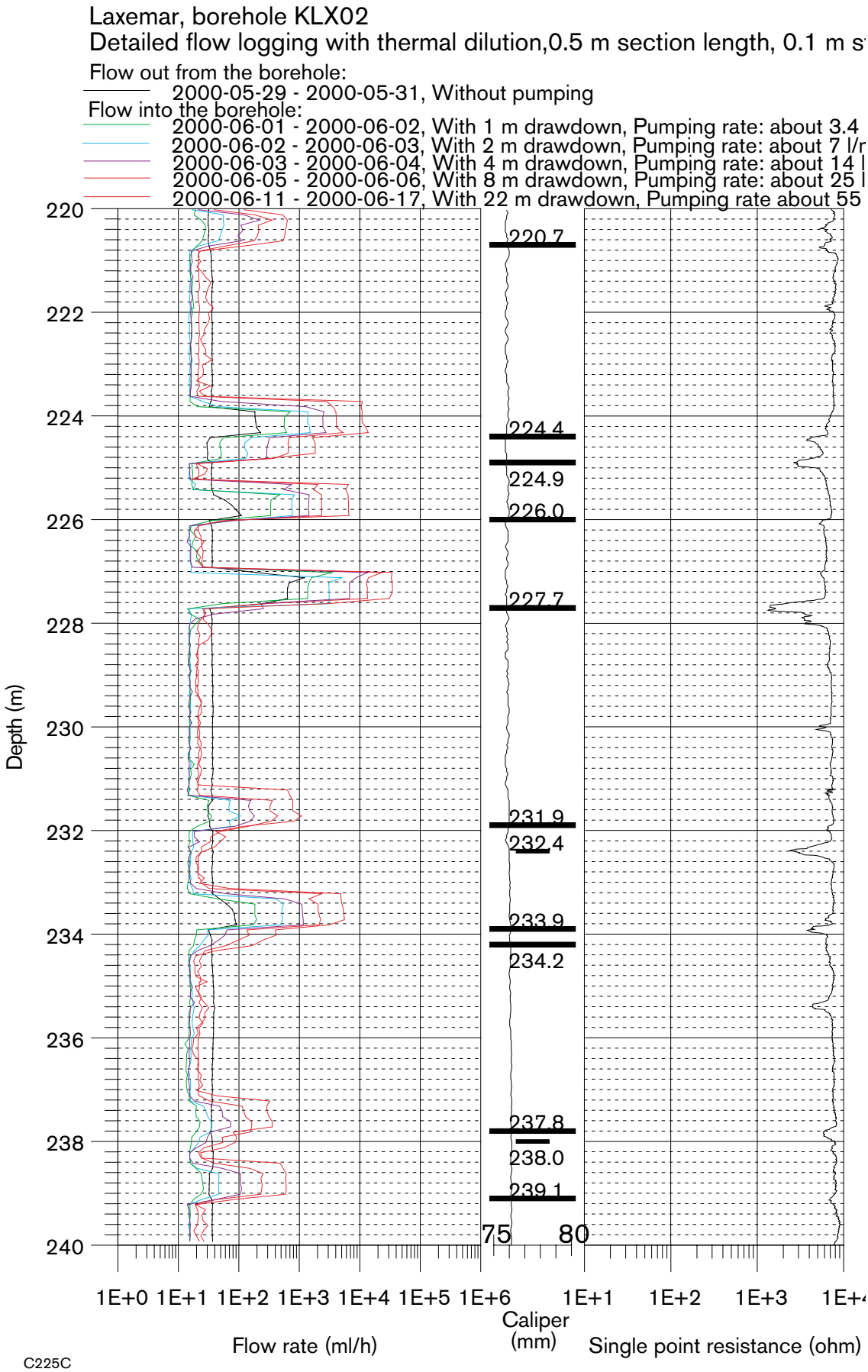
Laxemar, borehole KLX02
Detailed flow logging with thermal dilution,0.5 m section length, 0.1 m s
Flow out from the borehole:
2000-05-29 - 2000-05-31, Without pumping
Flow into the borehole:
2000-06-01 - 2000-06-02, With 1 m drawdown, Pumping rate: about 3.4
2000-06-02 - 2000-06-03, With 2 m drawdown, Pumping rate: about 7 l/r
2000-06-03 - 2000-06-04, With 4 m drawdown, Pumping rate: about 14 l
2000-06-05 - 2000-06-06, With 8 m drawdown, Pumping rate: about 25 l
2000-06-11 - 2000-06-17, With 22 m drawdown, Pumping rate about 55
Depth (m)
220
222
224
226
228
230
232
234
236
238
240
220.7
224.4
224.9
226.0
227.7
231.9
232.4
233.9
234.2
237.8
238.0
239.1
75
80
1E+0 1E+1 1E+2 1E+3 1E+4 1E+5 1E+6
1E+1 1E+2 1E+3 1E+4
Flow rate (ml/h)
Caliper (mm)
Single point resistance (ohm)
C225C

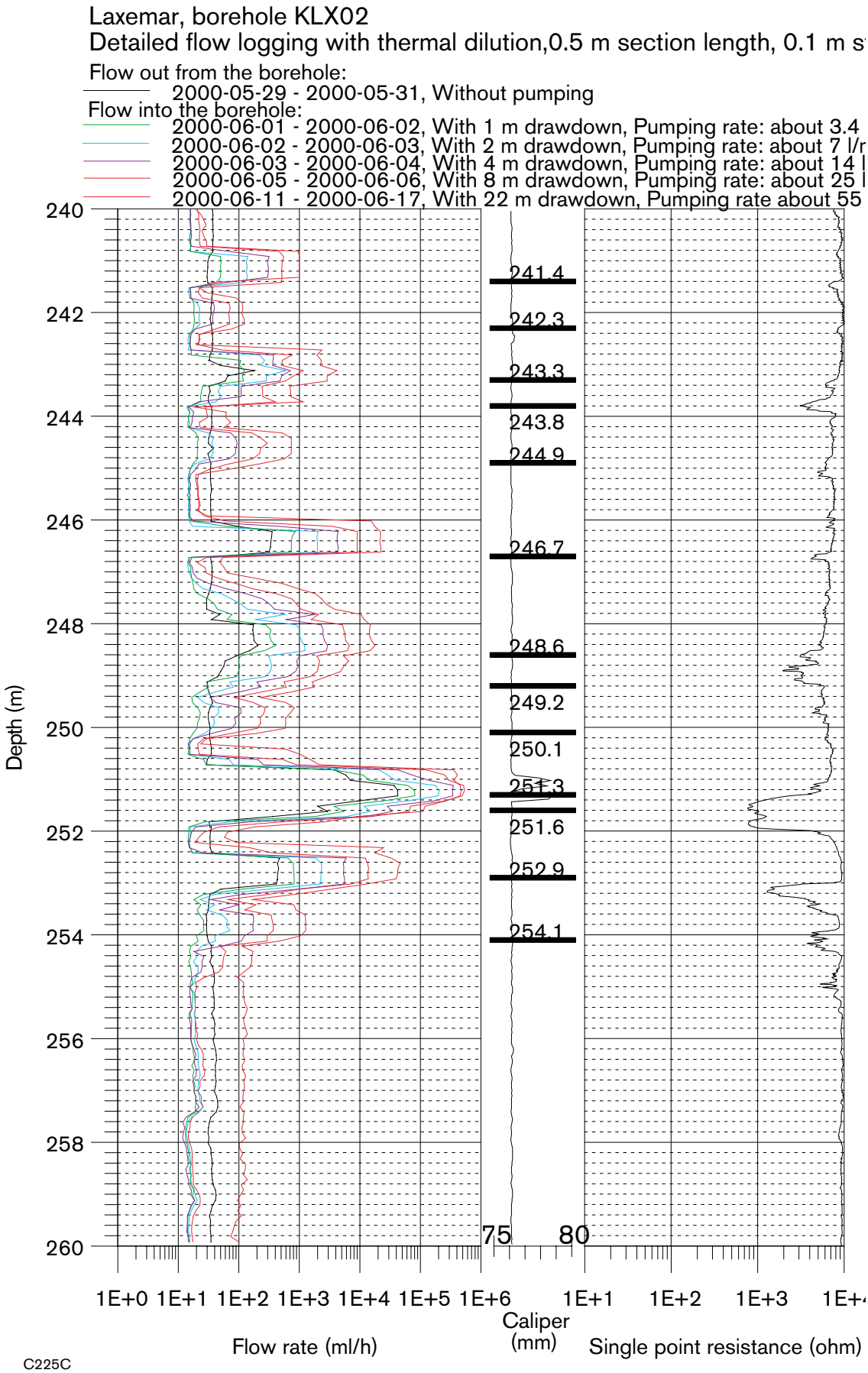
Laxemar, borehole KLX02
Detailed flow logging with thermal dilution,0.5 m section length, 0.1 m s
Flow out from the borehole:
2000-05-29 - 2000-05-31, Without pumping
Flow into the borehole:
2000-06-01 - 2000-06-02, With 1 m drawdown, Pumping rate: about 3.4
2000-06-02 - 2000-06-03, With 2 m drawdown, Pumping rate: about 7 l/r
2000-06-03 - 2000-06-04, With 4 m drawdown, Pumping rate: about 14 l
2000-06-05 - 2000-06-06, With 8 m drawdown, Pumping rate: about 25 l
2000-06-11 - 2000-06-17, With 22 m drawdown, Pumping rate about 55
Depth (m)
240
242
244
246
248
250
252
254
256
258
260
241.4
242.3
243.3
243.8
244.9
246.7
248.6
249.2
250.1
251.3
251.6
252.9
254.1
75
80
1E+0 1E+1 1E+2 1E+3 1E+4 1E+5 1E+6
1E+1 1E+2 1E+3 1E+4
Flow rate (ml/h)
Caliper (mm)
Single point resistance (ohm)
C225C

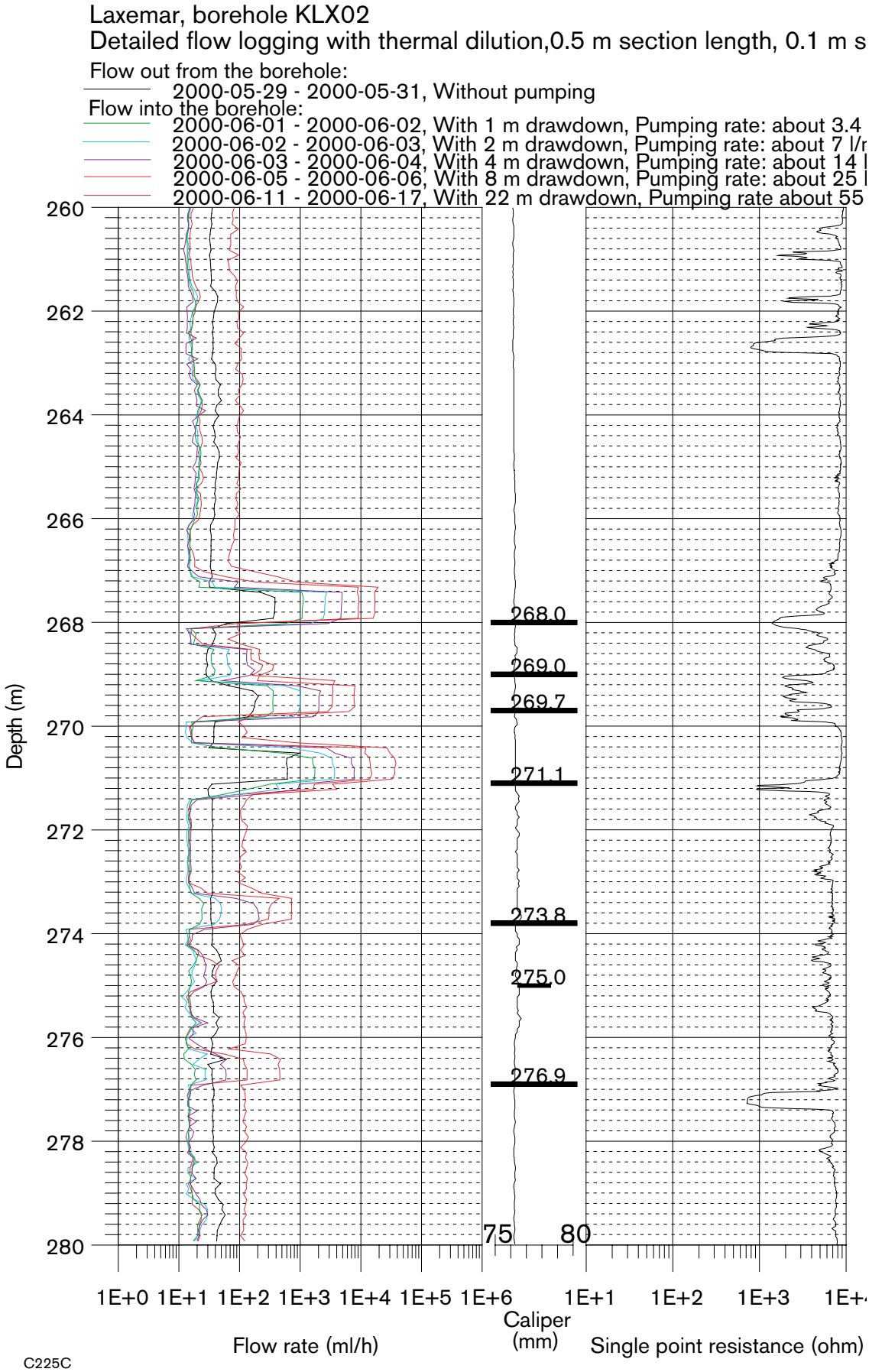
Laxemar, borehole KLX02
Detailed flow logging with thermal dilution,0.5 m section length, 0.1 m s
Flow out from the borehole:
2000-05-29 - 2000-05-31, Without pumping
Flow into the borehole:
2000-06-01 - 2000-06-02, With 1 m drawdown, Pumping rate: about 3.4
2000-06-02 - 2000-06-03, With 2 m drawdown, Pumping rate: about 7 l/r
2000-06-03 - 2000-06-04, With 4 m drawdown, Pumping rate: about 14 l
2000-06-05 - 2000-06-06, With 8 m drawdown, Pumping rate: about 25 l
2000-06-11 - 2000-06-17, With 22 m drawdown, Pumping rate about 55
Depth (m)
260
262
264
266
268
270
272
274
276
278
280
268.0
269.0
269.7
271.1
273.8
275.0
276.9
75
80
1E+0 1E+1 1E+2 1E+3 1E+4 1E+5 1E+6
Flow rate (ml/h)
Caliper (mm)
1E+1 1E+2 1E+3 1E+
Single point resistance (ohm)
C225C

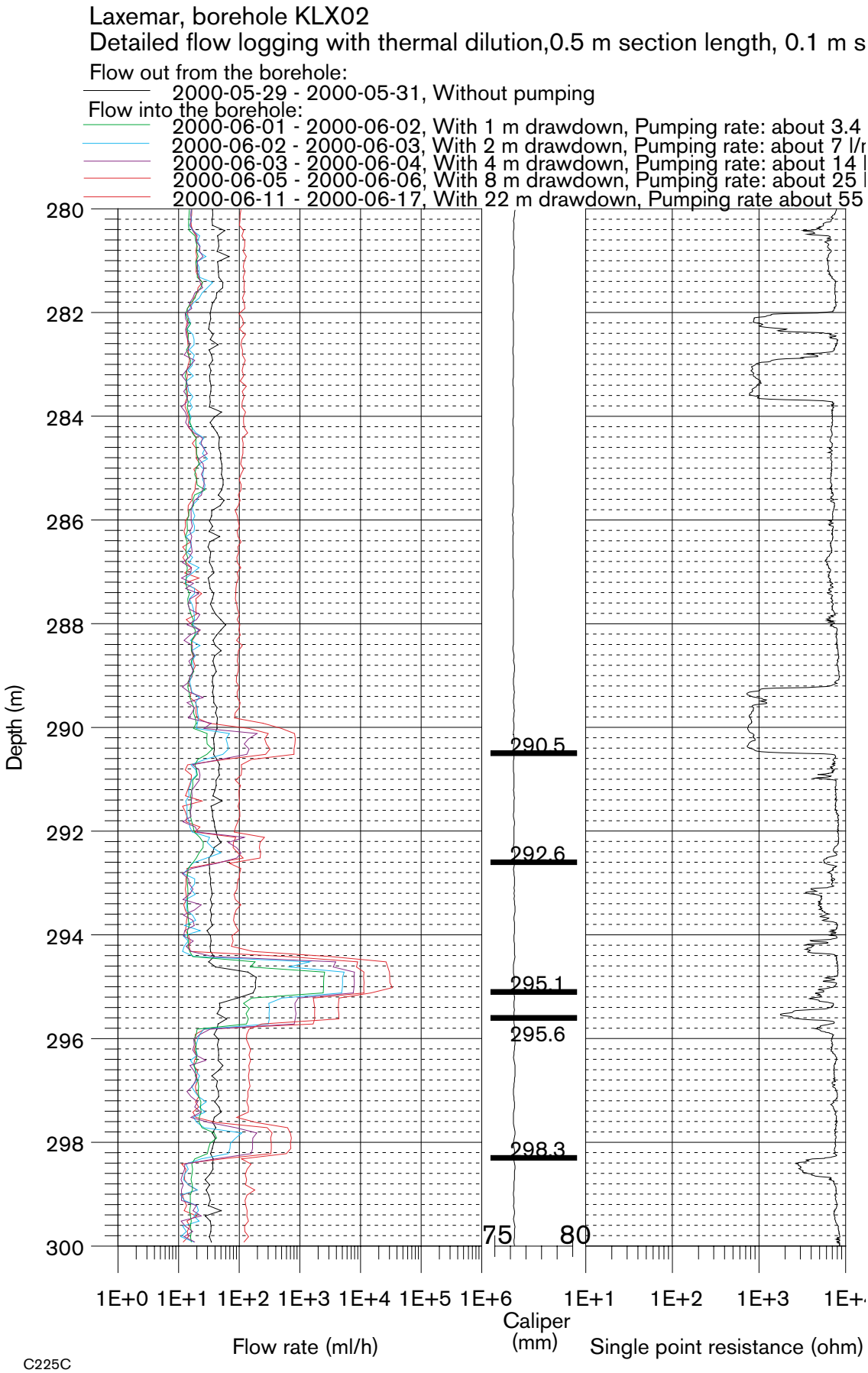
Laxemar, borehole KLX02
Detailed flow logging with thermal dilution,0.5 m section length, 0.1 m s
Flow out from the borehole:
2000-05-29 - 2000-05-31, Without pumping
Flow into the borehole:
2000-06-01 - 2000-06-02, With 1 m drawdown, Pumping rate: about 3.4
2000-06-02 - 2000-06-03, With 2 m drawdown, Pumping rate: about 7 l/r
2000-06-03 - 2000-06-04, With 4 m drawdown, Pumping rate: about 14 l
2000-06-05 - 2000-06-06, With 8 m drawdown, Pumping rate: about 25 l
2000-06-11 - 2000-06-17, With 22 m drawdown, Pumping rate about 55
Depth (m)
280
282
284
286
288
290
292
294
296
298
300
290.5
292.6
295.1
295.6
298.3
75
80
1E+0 1E+1 1E+2 1E+3 1E+4 1E+5 1E+6
1E+1 1E+2 1E+3 1E+
Caliper (mm)
Flow rate (ml/h)
Single point resistance (ohm)
C225C

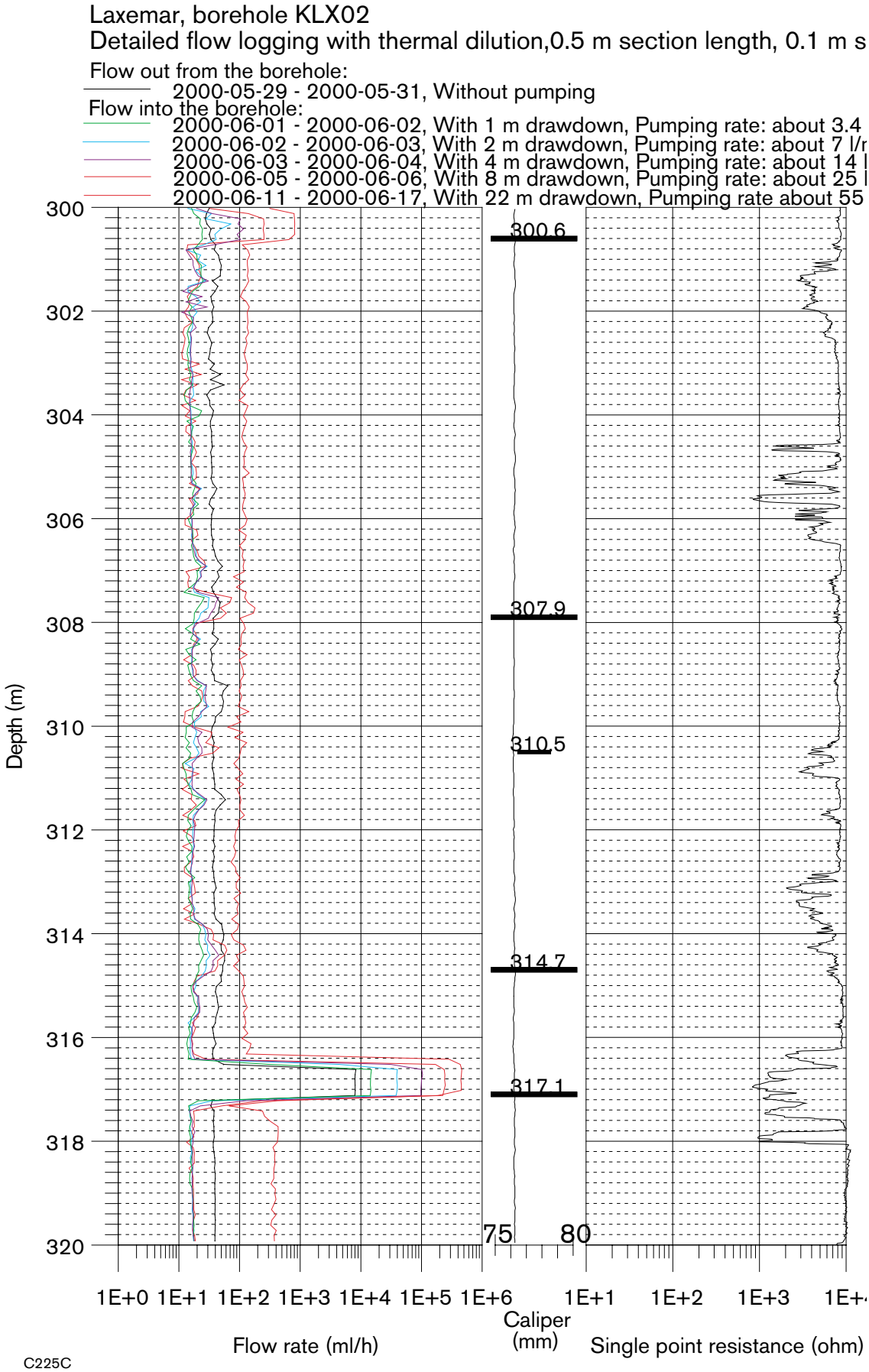
Laxemar, borehole KLX02
Detailed flow logging with thermal dilution,0.5 m section length, 0.1 m s
Flow out from the borehole:
2000-05-29 - 2000-05-31, Without pumping
Flow into the borehole:
2000-06-01 - 2000-06-02, With 1 m drawdown, Pumping rate: about 3.4
2000-06-02 - 2000-06-03, With 2 m drawdown, Pumping rate: about 7 l/r
2000-06-03 - 2000-06-04, With 4 m drawdown, Pumping rate: about 14 l
2000-06-05 - 2000-06-06, With 8 m drawdown, Pumping rate: about 25 l
2000-06-11 - 2000-06-17, With 22 m drawdown, Pumping rate about 55
Depth (m)
300
302
304
306
308
310
312
314
316
318
320
300.6
307.9
310.5
314.7
317.1
75
80
1E+0 1E+1 1E+2 1E+3 1E+4 1E+5 1E+6
Flow rate (ml/h)
Caliper
(mm)
1E+1 1E+2 1E+3 1E+
Single point resistance (ohm)
C225C

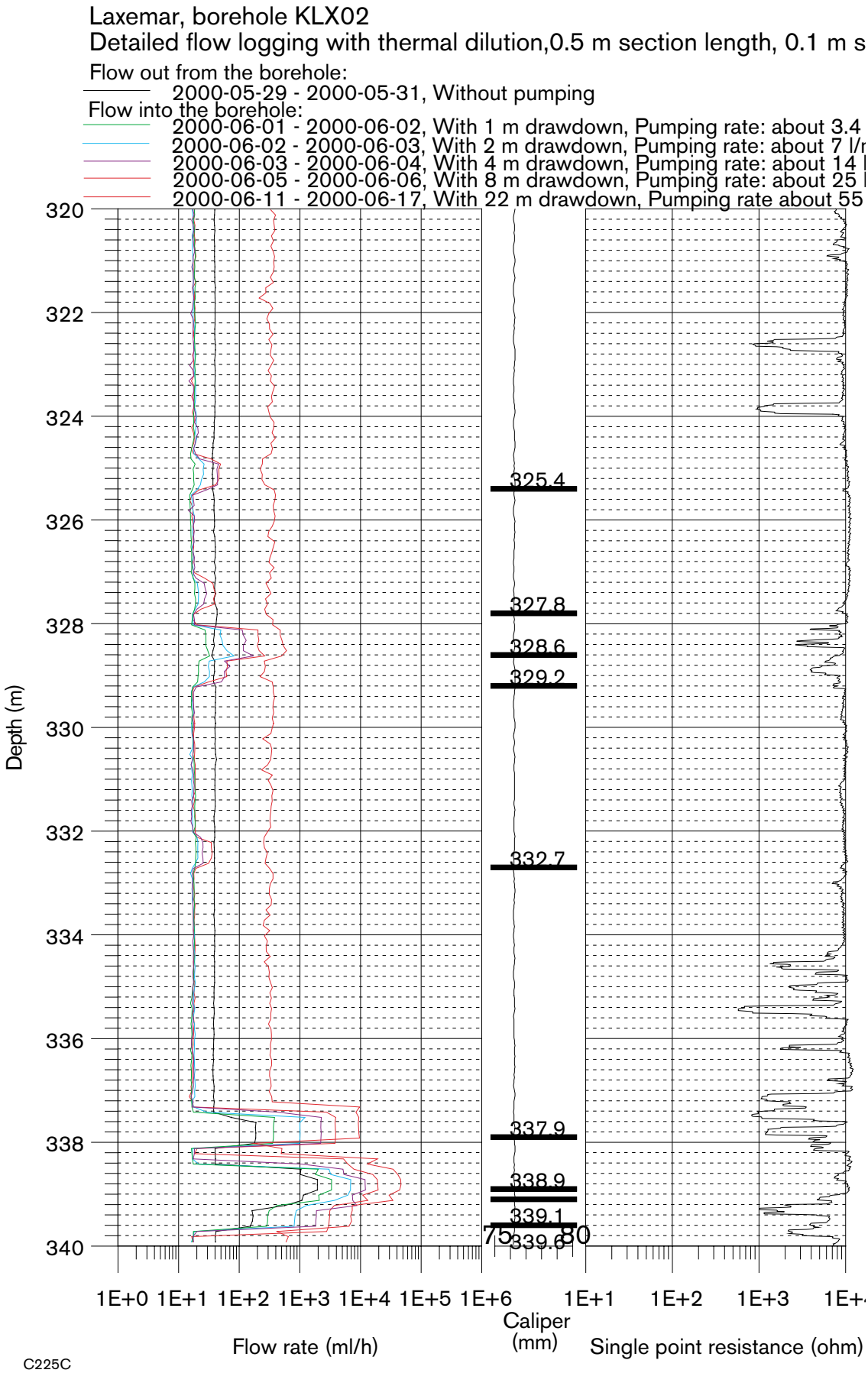
Laxemar, borehole KLX02
Detailed flow logging with thermal dilution,0.5 m section length, 0.1 m s
Flow out from the borehole:
2000-05-29 - 2000-05-31, Without pumping
Flow into the borehole:
2000-06-01 - 2000-06-02, With 1 m drawdown, Pumping rate: about 3.4
2000-06-02 - 2000-06-03, With 2 m drawdown, Pumping rate: about 7 l/r
2000-06-03 - 2000-06-04, With 4 m drawdown, Pumping rate: about 14 l
2000-06-05 - 2000-06-06, With 8 m drawdown, Pumping rate: about 25 l
2000-06-11 - 2000-06-17, With 22 m drawdown, Pumping rate about 55
320
322
324
326
328
330
332
334
336
338
340
Depth (m)
325.4
327.8
328.6
329.2
332.7
337.9
338.9
339.1
339.6
75
80
1E+0 1E+1 1E+2 1E+3 1E+4 1E+5 1E+6
1E+1 1E+2 1E+3 1E+
Flow rate (ml/h)
Caliper
(mm)
Single point resistance (ohm)
C225C

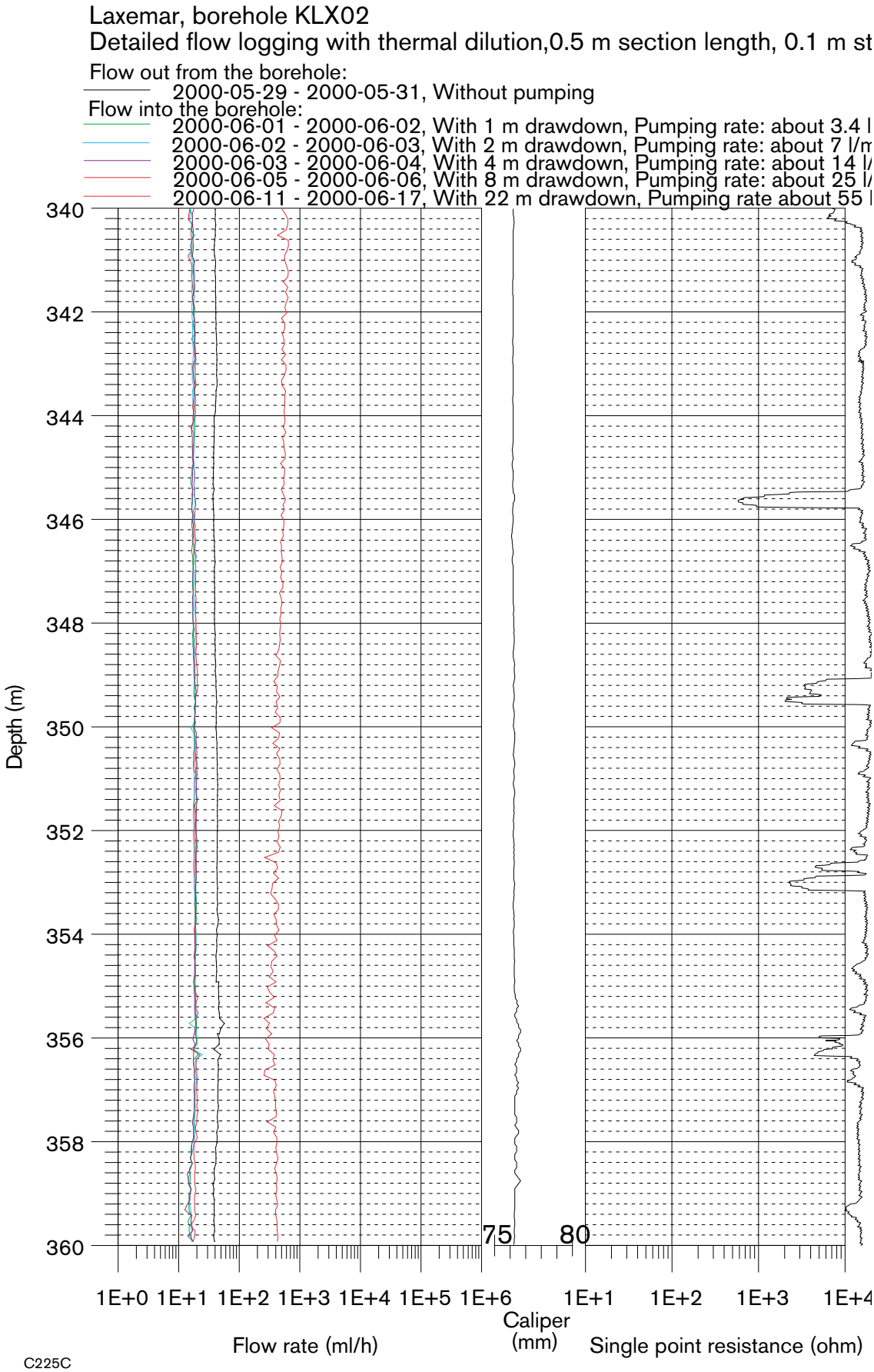
Laxemar, borehole KLX02
Detailed flow logging with thermal dilution,0.5 m section length, 0.1 m st
Flow out from the borehole:
2000-05-29 - 2000-05-31, Without pumping
Flow into the borehole:
2000-06-01 - 2000-06-02, With 1 m drawdown, Pumping rate: about 3.4 l
2000-06-02 - 2000-06-03, With 2 m drawdown, Pumping rate: about 7 l/m
2000-06-03 - 2000-06-04, With 4 m drawdown, Pumping rate: about 14 l/
2000-06-05 - 2000-06-06, With 8 m drawdown, Pumping rate: about 25 l/
2000-06-11 - 2000-06-17, With 22 m drawdown, Pumping rate about 55 l
Depth (m)
340
342
344
346
348
350
352
354
356
358
360
75
80
1E+0 1E+1 1E+2 1E+3 1E+4 1E+5 1E+6
1E+1 1E+2 1E+3 1E+4
Caliper (mm)
Flow rate (ml/h)
Single point resistance (ohm)
C225C

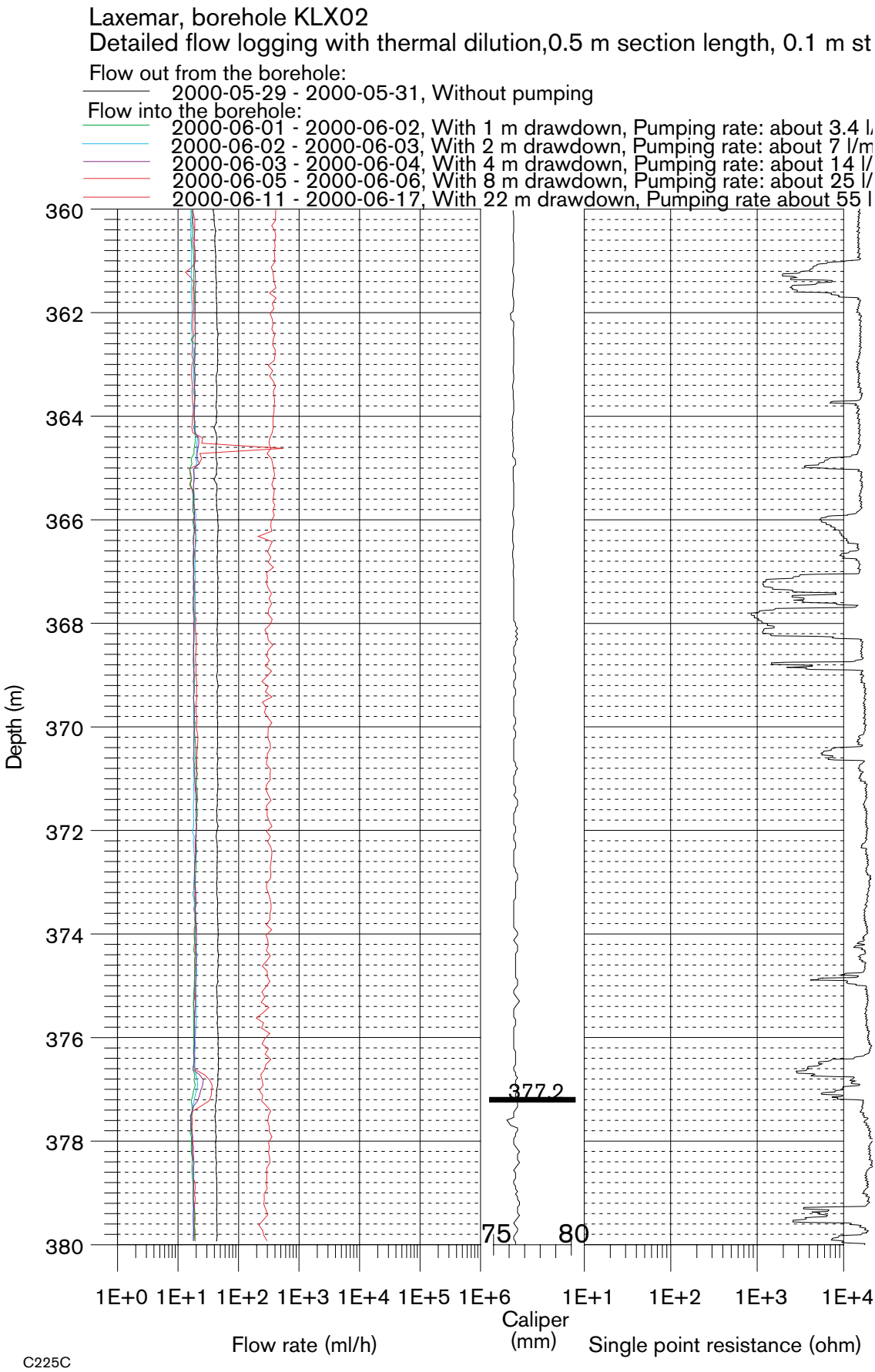
Laxemar, borehole KLX02
Detailed flow logging with thermal dilution,0.5 m section length, 0.1 m st
Flow out from the borehole:
2000-05-29 - 2000-05-31, Without pumping
Flow into the borehole:
2000-06-01 - 2000-06-02, With 1 m drawdown, Pumping rate: about 3.4 l
2000-06-02 - 2000-06-03, With 2 m drawdown, Pumping rate: about 7 l/m
2000-06-03 - 2000-06-04, With 4 m drawdown, Pumping rate: about 14 l/
2000-06-05 - 2000-06-06, With 8 m drawdown, Pumping rate: about 25 l/
2000-06-11 - 2000-06-17, With 22 m drawdown, Pumping rate about 55 l
Depth (m)
360
362
364
366
368
370
372
374
376
378
380
377.2
75
80
1E+0 1E+1 1E+2 1E+3 1E+4 1E+5 1E+6
1E+1 1E+2 1E+3 1E+4
Caliper (mm)
Flow rate (ml/h)
Single point resistance (ohm)
C225C

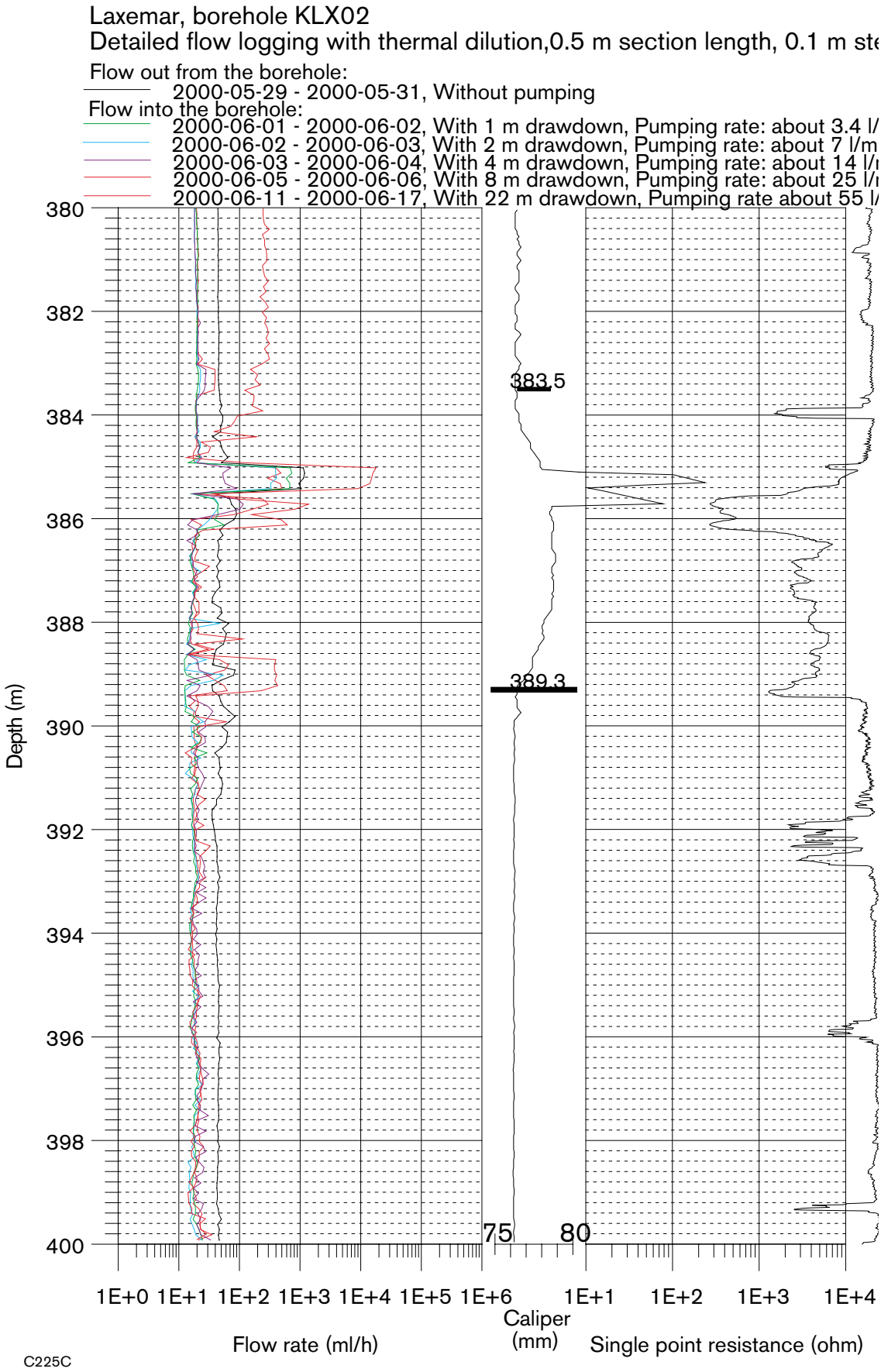
Laxemar, borehole KLX02
Detailed flow logging with thermal dilution,0.5 m section length, 0.1 m ste
Flow out from the borehole:
2000-05-29 - 2000-05-31, Without pumping
Flow into the borehole:
2000-06-01 - 2000-06-02, With 1 m drawdown, Pumping rate: about 3.4 l/
2000-06-02 - 2000-06-03, With 2 m drawdown, Pumping rate: about 7 l/m
2000-06-03 - 2000-06-04, With 4 m drawdown, Pumping rate: about 14 l/
2000-06-05 - 2000-06-06, With 8 m drawdown, Pumping rate: about 25 l/
2000-06-11 - 2000-06-17, With 22 m drawdown, Pumping rate about 55 l/
Depth (m)
380
382
384
386
388
390
392
394
396
398
400
383.5
389.3
75
80
1E+0 1E+1 1E+2 1E+3 1E+4 1E+5 1E+6
1E+1 1E+2 1E+3 1E+4
Flow rate (ml/h)
Caliper (mm)
Single point resistance (ohm)
C225C

Appendix 2

Borehole television (BIPS) characterisation

RecLength=Recorded length, AdjLength=Adjusted length

RecLength	AdjLength	Strike	Dip	Sort	Width	Form	Condition	Remark
205.873	206.106	6	22	Fracture	3	Planar	Dull	Quartz
206.353	206.594	260	9	Fracture	2	Undulating	Oxidized	Chlorite
206.387	206.629	300	22	Fracture	3	Planar	Oxidized	Chlorite
207.430	207.688	126	49	Fracture	4	Undulating	Dull	Chlorite
209.047	209.331	304	14	Fracture	3	Undulating	Oxidized	Calcite
209.140	209.425	138	75	Fracture	2	Irregular	Oxidized	Chlorite
209.230	209.517	159	26	Fracture	2	Undulating	Dull	Chlorite
209.271	209.558	204	17	Fracture	2	Undulating	Dull	Chlorite
211.794	212.121	119	77	Fracture	4	Undulating	Dull	Chlorite
213.374	213.726	104	85	Fracture	15	Undulating	Open	Chlorite
213.631	213.987	20	81	Fracture	18	Undulating	Open	Chlorite
214.448	214.817	126	79	Fracture	2	Irregular	Dull	Chlorite
214.587	214.958	134	79	Fracture	3	Undulating	Dull	Chlorite
214.854	215.230	261	24	Vein	29	Undulating	Dull	Fine.gran
214.912	215.289	137	66	Fracture	3	Planar	Dull	Chlorite
214.974	215.352	280	23	Vein	24	Undulating	Dull	Fine.gran
216.360	216.760	129	68	Fracture	3	Undulating	Cavities	Chlorite
217.804	218.226	118	78	Fracture	3	Irregular	Dull	Chlorite
219.052	219.494	17	80	Fracture	9	Undulating	Dull	Chlorite
219.530	219.980	286	6	Fracture	3	Undulating	Oxidized	Epidote
219.483	219.932	238	65	Fracture	2	Undulating	Dull	Chlorite
219.907	220.363	233	53	Fracture	3	Planar	Oxidized	Chlorite
220.118	220.577	253	69	Fracture	3	Undulating	Dull	Chlorite
220.376	220.839	255	59	Fracture	4	Undulating	Cavities	Chlorite
223.492	224.004	155	62	Fracture	2	Undulating	Oxidized	Chlorite
223.928	224.447	159	34	Fracture	4	Planar	Open	Chlorite
224.380	224.907	138	69	Fracture	4	Planar	Cavities	Chlorite
225.105	225.643	42	29	Vein	10	Planar	Dull	Fine.gran
225.512	226.056	202	25	Fracture	2	Undulating	Cavities	Chlorite
226.510	227.070	113	64	Fracture	3	Irregular	Dull	Chlorite
227.345	227.918	93	86	Fracture	14	Planar	Oxidized	Chlorite
231.301	231.937	292	54	Fracture	2	Planar	Dull	Chlorite
231.653	232.295	290	22	Fracture	1	Undulating	Dull	Chlorite
231.698	232.340	284	10	Fracture	12	Planar	Oxidized	Chlorite
231.752	232.395	224	9	Fracture	17	Undulating	Oxidized	Quartz
233.191	233.857	137	56	Fracture	4	Undulating	Cavities	Chlorite
233.420	234.090	263	2	Vein	34	Irregular	Dull	Chlorite
236.343	237.059	126	85	Vein	19	Undulating	Dull	Chlorite
236.684	237.405	277	49	Vein	26	Undulating	Dull	Fine.gran
237.056	237.783	163	64	Fracture	6	Irregular	Cavities	Chlorite
237.341	238.073	174	53	Fracture	1	Undulating	Cavities	Chlorite
240.558	241.341	281	42	Fracture	2	Planar	Cavities	Chlorite
241.771	242.573	125	26	Vein	5	Undulating	Oxidized	Granite
242.477	243.290	229	45	Fracture	2	Undulating	Cavities	Chlorite
242.719	243.536	142	71	Fracture	7	Undulating	Cavities	Chlorite
244.056	244.894	279	69	Fracture	2	Undulating	Dull	Chlorite
245.735	246.600	136	45	Fracture	4	Undulating	Open	Chlorite
247.608	248.502	121	70	Fracture	3	Undulating	Cavities	Chlorite
247.771	248.668	301	79	Fracture	5	Irregular	Cavities	Chlorite
248.371	249.277	213	70	Fracture	5	Undulating	Dull	Chlorite
248.936	249.851	237	77	Fracture	5	Planar	Cavities	Chlorite
250.535	251.476	45	89	Fracture	5	Undulating	Oxidized	Chlorite
250.549	251.490	302	78	Fracture	14	Undulating	Open	Chlorite

RecLength	AdjLength	Strike	Dip	Sort	Width	Form	Condition	Remark
252.099	253.064	285	74	Fracture	7	Undulating	Open	Chlorite
252.947	253.926	298	75	Fracture	6	Undulating	Cavities	Chlorite
253.583	254.572	292	74	Fracture	2	Irregular	Cavities	Chlorite
255.826	256.851	137	79	Vein	15	Undulating	Dull	Pegmatite
257.130	258.175	135	66	Vein	13	Undulating	Dull	Pegmatite
257.650	258.703	313	17	Fracture	2	Undulating	Oxidized	Chlorite
259.250	260.329	321	32	Fracture	1	Undulating	Oxidized	Chlorite
260.706	261.808	357	9	Vein	28	Undulating	Oxidized	Pegmatite
260.771	261.874	359	12	Vein	10	Undulating	Oxidized	Pegmatite
262.232	263.358	327	21	Fracture	2	Undulating	Oxidized	Chlorite
262.928	264.065	90	87	Fracture	7	Irregular	Oxidized	Fine.gran
265.871	267.055	283	71	Vein	13	Undulating	Oxidized	Pegmatite
266.168	267.356	273	72	Fracture	4	Irregular	Cavities	Chlorite
266.586	267.781	285	58	Fracture	3	Undulating	Open	Chlorite
266.677	267.873	275	32	Fracture	4	Undulating	Oxidized	Chlorite
266.738	267.935	270	22	Fracture	2	Planar	Oxidized	Chlorite
267.044	268.246	257	23	Fracture	1	Undulating	Oxidized	Chlorite
267.622	268.833	265	21	Fracture	2	Undulating	Cavities	Chlorite
267.774	268.988	286	14	Fracture	3	Undulating	Oxidized	Chlorite
267.829	269.044	313	38	Fracture	2	Undulating	Cavities	Chlorite
267.947	269.164	286	33	Fracture	4	Undulating	Open	Chlorite
268.034	269.252	277	35	Fracture	5	Irregular	Cavities	Chlorite
268.317	269.539	275	59	Fracture	7	Undulating	Open	Chlorite
269.638	270.881	121	57	Fracture	5	Undulating	Open	Chlorite
270.890	272.153	218	18	Fracture	1	Planar	Dull	Chlorite
272.975	274.271	146	54	Vein	16	Undulating	Oxidized	Pegmatite
275.296	276.629	268	19	Fracture	5	Planar	Open	Chlorite
276.715	278.071	281	37	Fracture	3	Planar	Oxidized	Chlorite
278.474	279.857	23	23	Fracture	1	Planar	Oxidized	Chlorite
279.043	280.435	8	35	Fracture	1	Planar	Oxidized	Chlorite
279.633	281.035	0	10	Fracture	1	Planar	Oxidized	Chlorite
279.914	281.320	44	32	Fracture	1	Planar	Oxidized	Chlorite
281.366	282.795	287	29	Fracture	1	Planar	Oxidized	Chlorite
281.713	283.148	7	26	Fracture	1	Planar	Oxidized	Chlorite
282.460	283.907	296	9	Vein	7	Undulating	Oxidized	Pegmatite
282.600	284.049	2	50	Fracture	1	Undulating	Oxidized	Calcite
283.496	284.959	239	2	Fracture	1	Planar	Oxidized	Calcite
284.917	286.402	61	38	Vein	19	Undulating	Dull	Chlorite
285.907	287.408	93	16	Vein	6	Undulating	Oxidized	Pegmatite
286.352	287.860	87	10	Fracture	1	Planar	Oxidized	Chlorite
288.517	290.060	224	30	Vein	25	Irregular	Dull	Chlorite
288.937	290.486	253	46	Fracture	9	Undulating	Dull	Chlorite
289.008	290.558	287	67	Fracture	13	Irregular	Dull	Chlorite
289.281	290.836	104	73	Fracture	6	Undulating	Oxidized	Calcite
289.601	291.161	123	74	Vein	17	Irregular	Oxidized	Chlorite
293.193	294.699	30	44	Vein	38	Undulating	Dull	Fine.gran
295.340	296.784	104	65	Fracture	2	Undulating	Cavities	Chlorite
295.468	296.909	101	52	Fracture	1	Undulating	Cavities	Chlorite
295.527	296.966	110	41	Fracture	3	Undulating	Cavities	Chlorite
296.082	297.505	118	55	Fracture	3	Planar	Cavities	Chlorite
296.566	297.975	111	61	Fracture	4	Planar	Oxidized	Chlorite
299.333	300.662	300	27	Fracture	4	Planar	Dull	Quartz
300.813	302.099	275	22	Fracture	1	Undulating	Oxidized	Calcite
300.901	302.184	106	49	Fracture	2	Planar	Cavities	Chlorite
305.929	307.066	314	14	Vein	4	Planar	Oxidized	Pegmatite
308.311	309.379	307	16	Vein	8	Planar	Oxidized	Pegmatite
308.499	309.562	272	20	Vein	10	Planar	Oxidized	Pegmatite
310.636	311.637	299	62	Fracture	3	Planar	Cavities	Chlorite
310.684	311.684	36	21	Vein	134	Undulating	Dull	Fine.gran
310.825	311.821	245	66	Fracture	11	Irregular	Oxidized	Chlorite
311.161	312.147	17	16	Vein	120	Undulating	Dull	Fine.gran
311.545	312.520	62	46	Vein	114	Undulating	Oxidized	Fine.gran

RecLength	AdjLength	Strike	Dip	Sort	Width	Form	Condition	Remark
312.390	313.340	84	22	Fracture	3	Undulating	Dull	Chlorite
312.680	313.622	25	19	Fracture	2	Undulating	Dull	Chlorite
314.706	315.589	301	65	Fracture	1	Planar	Cavities	Chlorite
316.008	316.853	111	18	Fracture	2	Planar	Dull	Chlorite
316.868	317.688	179	48	Fracture	1	Planar	Oxidized	Calcite
317.017	317.833	295	54	Fracture	8	Planar	Open	Chlorite
318.808	319.572	347	62	Fracture	1	Planar	Oxidized	Chlorite
320.233	320.956	19	41	Fracture	12	Planar	Dull	Chlorite
320.690	321.400	274	22	Fracture	1	Planar	Oxidized	Chlorite
323.241	323.877	214	27	Vein	7	Planar	Dull	Pegmatite
325.500	326.070	25	76	Fracture	2	Planar	Dull	Chlorite
327.390	327.905	21	20	Fracture	3	Planar	Cavities	Calcite
327.176	327.698	38	16	Vein	483	Undulating	Dull	Fine.gran
328.567	329.048	196	70	Fracture	3	Irregular	Cavities	Chlorite
328.451	328.936	277	73	Fracture	3	Irregular	Cavities	Chlorite
328.738	329.214	278	60	Fracture	2	Planar	Cavities	Chlorite
329.067	329.534	335	11	Vein	15	Planar	Dull	Chlorite
330.725	331.144	291	61	Fracture	1	Irregular	Dull	Chlorite
330.955	331.367	243	61	Fracture	3	Irregular	Dull	Chlorite
332.156	332.533	281	35	Vein	6	Undulating	Dull	Chlorite
332.194	332.570	281	38	Vein	10	Undulating	Dull	Chlorite
334.030	334.353	331	10	Vein	7	Undulating	Dull	Chlorite
334.405	334.717	154	38	Fracture	2	Planar	Oxidized	Chlorite
337.172	337.404	28	35	Vein	30	Planar	Oxidized	Pegmatite
337.484	337.707	268	36	Fracture	4	Irregular	Cavities	Chlorite
337.739	337.955	186	18	Fracture	1	Planar	Oxidized	Calcite
337.816	338.029	64	25	Alteration	0	Undulating	Oxidized	Granite
338.000	338.208	209	12	Fracture	1	Planar	Oxidized	Chlorite
338.054	338.260	225	3	Fracture	1	Undulating	Oxidized	Chlorite
338.123	338.327	241	3	Fracture	2	Undulating	Oxidized	Chlorite
338.203	338.405	130	15	Alteration	0	Undulating	Dull	Granite
338.421	338.617	230	19	Fracture	4	Undulating	Oxidized	Chlorite
338.471	338.665	241	20	Fracture	6	Undulating	Open	Chlorite
338.632	338.822	240	32	Fracture	8	Undulating	Open	Chlorite
338.781	338.966	296	73	Fracture	2	Irregular	Cavities	Chlorite
338.605	338.795	241	35	Vein	542	Undulating	Dull	Chlorite
338.968	339.148	169	7	Fracture	1	Planar	Cavities	Chlorite
339.104	339.280	253	47	Fracture	3	Undulating	Open	Chlorite
339.369	339.537	285	75	Fracture	4	Irregular	Cavities	Chlorite
340.937	341.094	250	46	Vein	10	Undulating	Dull	Chlorite
341.289	341.449	104	79	Vein	9	Undulating	Dull	Chlorite
343.462	343.638	97	70	Vein	14	Undulating	Dull	Fine.gran
344.920	345.107	270	14	Vein	7	Undulating	Dull	Fine.gran
345.772	345.965	295	44	Fracture	1	Planar	Dull	Chlorite
345.486	345.677	93	11	Vein	862	Undulating	Dull	Fine.gran
346.927	347.129	78	68	Vein	8	Planar	Oxidized	Pegmatite
347.816	348.025	108	28	Vein	59	Undulating	Dull	Fine.gran
349.105	349.323	187	11	Vein	14	Undulating	Dull	Fine.gran
349.566	349.788	195	32	Vein	34	Undulating	Dull	Chlorite
349.736	349.959	60	36	Vein	8	Undulating	Dull	Chlorite
349.872	350.096	231	34	Vein	15	Irregular	Dull	Chlorite
350.049	350.274	332	40	Fracture	2	Planar	Oxidized	Chlorite
350.040	350.265	227	42	Vein	56	Undulating	Dull	Chlorite
350.420	350.648	77	40	Vein	6	Planar	Dull	Pegmatite
353.594	353.846	234	29	Vein	5	Irregular	Dull	Chlorite
354.071	354.327	172	2	Vein	7	Undulating	Dull	Fine.gran
354.681	354.941	333	21	Contact	0	Undulating	Dull	Chlorite
354.807	355.068	295	14	Fracture	2	Planar	Dull	Calcite
354.860	355.121	305	13	Fracture	1	Planar	Dull	Calcite
354.934	355.196	310	11	Fracture	2	Planar	Dull	Calcite
355.009	355.272	299	26	Fracture	2	Planar	Dull	Calcite
355.108	355.371	290	31	Fracture	36	Network	Dull	Fine.gran

RecLength	AdjLength	Strike	Dip	Sort	Width	Form	Condition	Remark
355.623	355.890	16	9	Fracture	3	Undulating	Dull	Calcite
355.675	355.943	41	18	Fracture	4	Network	Dull	Calcite
355.732	356.000	19	10	Fracture	2	Undulating	Dull	Calcite
355.928	356.197	43	53	Fracture	6	Undulating	Dull	Calcite
356.143	356.414	26	30	Fracture	6	Network	Dull	Calcite
356.222	356.494	59	28	Fracture	4	Network	Dull	Calcite
356.346	356.619	49	46	Fracture	9	Network	Dull	Calcite
356.498	356.772	54	36	Fracture	5	Network	Dull	Calcite
356.608	356.883	10	33	Fracture	7	Undulating	Dull	Calcite
356.773	357.049	29	51	Fracture	7	Undulating	Dull	Calcite
356.895	357.172	14	22	Fracture	4	Undulating	Dull	Calcite
357.282	357.562	82	31	Fracture	4	Undulating	Dull	Calcite
357.638	357.920	77	26	Vein	102	Undulating	Dull	Granite
357.752	358.035	81	30	Vein	30	Undulating	Dull	Granite
357.911	358.195	102	30	Vein	50	Undulating	Dull	Granite
358.118	358.404	79	23	Contact	0	Undulating	Oxidized	Granite
358.206	358.493	325	46	Fracture	2	Undulating	Oxidized	Epidote
360.116	360.417	337	26	Vein	9	Planar	Oxidized	Pegmatite
360.645	360.950	26	13	Vein	5	Undulating	Dull	Chlorite
361.070	361.378	333	17	Vein	9	Undulating	Oxidized	Pegmatite
362.614	362.934	316	14	Vein	8	Undulating	Oxidized	Pegmatite
363.546	363.873	280	13	Vein	181	Planar	Dull	Chlorite
363.712	364.040	288	12	Fracture	2	Irregular	Cavities	Calcite
364.819	365.155	259	72	Fracture	3	Irregular	Dull	Chlorite
367.148	367.502	188	37	Vein	12	Undulating	Oxidized	Pegmatite
367.698	368.056	321	19	Fracture	2	Planar	Dull	Quartz
368.591	368.955	257	11	Vein	12	Planar	Dull	Chlorite
368.741	369.107	334	23	Vein	28	Undulating	Oxidized	Pegmatite
369.648	370.020	200	16	Vein	24	Planar	Oxidized	Pegmatite
370.791	371.172	295	49	Vein	37	Irregular	Dull	Chlorite
371.372	371.757	119	40	Vein	39	Planar	Dull	Pegmatite
371.805	372.194	316	22	Vein	8	Undulating	Oxidized	Pegmatite
372.058	372.448	22	35	Vein	11	Undulating	Oxidized	Pegmatite
372.715	373.110	210	21	Vein	16	Planar	Dull	Chlorite
374.324	374.731	316	16	Vein	3	Planar	Oxidized	Pegmatite
375.772	376.190	255	61	Vein	9	Planar	Dull	Chlorite
375.991	376.411	13	28	Fracture	0	Undulating	Oxidized	Chlorite
376.015	376.435	4	32	Fracture	1	Planar	Oxidized	Chlorite
376.102	376.523	37	32	Fracture	0	Planar	Oxidized	Chlorite
376.277	376.699	322	15	Fracture	8	Planar	Oxidized	Pegmatite
376.574	376.998	251	54	Fracture	2	Undulating	Dull	Chlorite
376.892	377.319	283	36	Vein	5	Irregular	Dull	Chlorite
377.279	377.709	315	32	Fracture	3	Planar	Oxidized	Pegmatite
377.389	377.819	340	22	Vein	4	Planar	Oxidized	Pegmatite
377.596	378.028	328	13	Fracture	3	Planar	Oxidized	Pegmatite
377.841	378.275	39	22	Fracture	0	Planar	Oxidized	Chlorite
377.985	378.420	223	19	Vein	16	Irregular	Dull	Chlorite
378.333	378.770	117	4	Fracture	30	Undulating	Dull	Chlorite
378.457	378.895	30	31	Fracture	8	Undulating	Oxidized	Chlorite
378.816	379.257	175	53	Fracture	1	Undulating	Oxidized	Chlorite
379.974	380.424	56	11	Fracture	3	Planar	Oxidized	Calcite
381.554	382.016	99	50	Vein	10	Undulating	Oxidized	Pegmatite
381.983	382.448	181	56	Fracture	45	Undulating	Oxidized	Chlorite
382.039	382.504	133	47	Vein	12	Undulating	Oxidized	Pegmatite
382.842	383.313	205	22	Fracture	1	Undulating	Oxidized	Chlorite
383.086	383.559	45	39	Contact	0	Planar	Dull	Chlorite
383.672	384.150	346	37	Fracture	4	Undulating	Open	Calcite
383.939	384.419	0	34	Fracture	2	Undulating	Open	Calcite
384.177	384.658	355	65	Fracture	33	Planar	Open	Calcite
384.322	384.804	312	54	Fracture	1	Planar	Cavities	Calcite
384.523	385.007	20	28	Fracture	2	Planar	Cavities	Calcite
384.820	385.306	347	27	Vein	48	Planar	Dull	Calcite

RecLength	AdjLength	Strike	Dip	Sort	Width	Form	Condition	Remark
385.080	385.568	348	53	Fracture	1	Planar	Dull	Calcite
385.315	385.805	343	46	Fracture	3	Planar	Dull	Calcite
385.467	385.958	42	65	Fracture	1	Planar	Cavities	Calcite
385.537	386.029	150	50	Fracture	1	Planar	Weathered	Calcite
385.808	386.302	12	75	Fracture	1	Planar	Dull	Calcite
386.743	387.244	339	45	Fracture	1	Planar	Dull	Calcite
387.064	387.567	181	47	Fracture	2	Planar	Cavities	Calcite
387.315	387.820	45	55	Contact	0	Planar	Dull	Granite
387.300	387.805	37	54	Fracture	3	Planar	Open	Calcite
387.852	388.361	46	58	Vein	9	Planar	Dull	Pegmatite
389.698	390.221	46	48	Fracture	4	Planar	Dull	Quartz
390.291	390.818	258	49	Vein	17	Planar	Dull	Fine.gran
390.710	391.240	276	42	Vein	17	Undulating	Dull	Fine.gran
390.968	391.500	54	49	Vein	52	Undulating	Dull	Pegmatite
394.014	394.569	309	18	Fracture	2	Planar	Dull	Chlorite
394.903	395.465	279	37	Fracture	7	Undulating	Dull	Chlorite
395.017	395.580	279	19	Fracture	2	Undulating	Dull	Chlorite
395.522	396.088	31	40	Vein	16	Planar	Dull	Pegmatite
396.029	396.599	46	15	Fracture	1	Planar	Oxidized	Calcite
396.167	396.738	84	16	Fracture	1	Planar	Oxidized	Chlorite
398.338	398.926	289	16	Fracture	1	Planar	Oxidized	Calcite
399.318	399.913	254	25	Vein	59	Undulating	Oxidized	Pegmatite

Appendix 3

Correlation table between Borehole television (BIPS) and flow logging

BIPS Correlation Class 1 = Uncertain, 2 = Medium 3 = Certain

Note	Flow ml/h	FlowSpot	RecLength	AdjLength	Strike	Dip	Sort	Width	Condition	Class
	2964	212.0	211.794	212.121	119	77	Fracture	4	Cavities	3
	158662	213.3	213.374	213.726	104	85	Fracture	15	Open	3
	16757	214.0	213.631	213.987	20	81	Fracture	18	Open	1
	5031	215.2	214.912	215.289	137	66	Fracture	3	Cavities	3
	302	216.7	216.360	216.760	129	68	Fracture	3	Cavities	3
	572	220.7	220.376	220.839	255	59	Fracture	4	Cavities	3
	12542	224.4	223.928	224.447	159	34	Fracture	4	Open	3
	1823	224.9	224.380	224.907	138	69	Fracture	4	Cavities	3
	6625	226.0	225.512	226.056	202	25	Fracture	2	Cavities	3
	30680	227.7	227.345	227.918	93	86	Fracture	14	Oxidized	3
	778	231.9	231.301	231.937	292	54	Fracture	2	Dull	2
	38	232.4	231.752	232.395	224	9	Fracture	17	Oxidized	3
	5337	233.9	233.191	233.857	137	56	Fracture	4	Cavities	3
	166	234.2	233.420	234.090	263	2	Vein	34	Dull	3
	359	237.8	237.056	237.783	163	64	Fracture	6	Cavities	3
	86	238.0	237.341	238.073	174	53	Fracture	1	Cavities	3
	990	241.4	240.558	241.341	281	42	Fracture	2	Cavities	3
	121	242.3	241.771	242.573	125	26	Vein	5	Oxidized	1
	2870	243.3	242.477	243.290	229	45	Fracture	2	Cavities	2
	714	243.8	242.719	243.536	142	71	Fracture	7	Cavities	2
	733	244.9	244.056	244.894	279	69	Fracture	2	Dull	2
	22150	246.7	245.735	246.600	136	45	Fracture	4	Open	3
	15479	248.6	247.608	248.502	121	70	Fracture	3	Cavities	3
	1623	249.2	248.371	249.277	213	70	Fracture	5	Dull	3
	578	250.1	248.936	249.851	237	77	Fracture	5	Cavities	1
	458764	251.3	250.535	251.476	45	89	Fracture	5	Oxidized	3
	111455	251.6	250.549	251.490	302	78	Fracture	14	Open	3
	41867	252.9	252.099	253.064	285	74	Fracture	7	Open	3
	1269	254.1	252.947	253.926	298	75	Fracture	6	Cavities	3
	16905	268.0	266.586	267.781	285	58	Fracture	3	Open	2
	213	269.0	267.622	268.833	265	21	Fracture	2	Cavities	3
	7977	269.7	268.317	269.539	275	59	Fracture	7	Open	3
	36168	271.1	269.638	270.881	121	57	Fracture	5	Open	3
	715	273.8	270.890	272.153	218	18	Fracture	1	Dull	1
B	0	275.0	272.975	274.271	146	54	Vein	16	Oxidized	1
	462	276.9	275.296	276.629	268	19	Fracture	5	Open	1
	796	290.5	289.008	290.558	287	67	Fracture	13	Dull	3
	219	292.6	293.193	294.699	30	44	Vein	38	Dull	1
	30324	295.1	295.527	296.966	110	41	Fracture	3	Cavities	3
	4393	295.6	296.082	297.505	118	55	Fracture	3	Cavities	3
	698	298.3	299.333	300.662	300	27	Fracture	4	Dull	1
	801	300.6	300.901	302.184	106	49	Fracture	2	Cavities	3
B	0	307.9	308.311	309.379	307	16	Vein	8	Oxidized	3
B	0	310.5	310.636	311.637	299	62	Fracture	3	Cavities	3
B	0	314.7	314.706	315.589	301	65	Fracture	1	Cavities	2
	452519	317.1	317.017	317.833	295	54	Fracture	8	Open	1
B	0	325.4	325.500	326.070	25	76	Fracture	2	Dull	3
B	0	327.8	327.390	327.905	21	20	Fracture	3	Cavities	1
B	0	328.6	328.451	328.936	277	73	Fracture	3	Cavities	3
B	0	329.2	329.067	329.534	335	11	Vein	15	Dull	3
B	0	332.7	332.194	332.570	281	38	Vein	10	Dull	1
	9576	337.9	337.484	337.707	268	36	Fracture	4	Cavities	1
	12983	338.9	338.471	338.665	241	20	Fracture	6	Open	3

Note	Flow ml/h	FlowSpot	RecLength	AdjLength	Strike	Dip	Sort	Width	Condition	Class
	34185	339.1	338.632	338.822	240	32	Fracture	8	Open	3
	717	339.6	339.104	339.280	253	47	Fracture	3	Open	3
B	0	377.2	376.892	377.319	283	36	Vein	5	Dull	2
B	0	383.5	383.086	383.559	45	39	Contact	0	Dull	3
U	c. 15000?	385.0	384.177	384.658	355	65	Fracture	33	Open	3
	375	389.3	387.300	387.805	37	54	Fracture	3	Open	1

B = below measurement limit
U = uncertain flow anomaly

Appendix 4

BIPS images of selected fractures

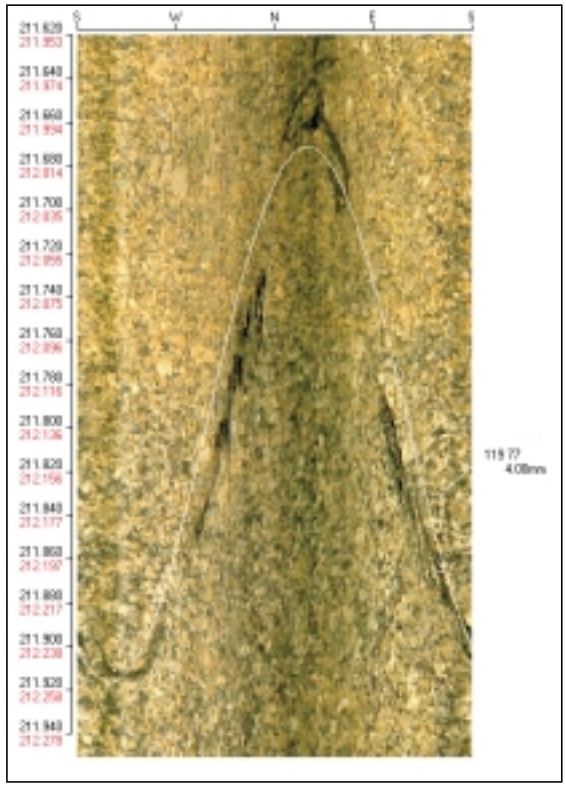

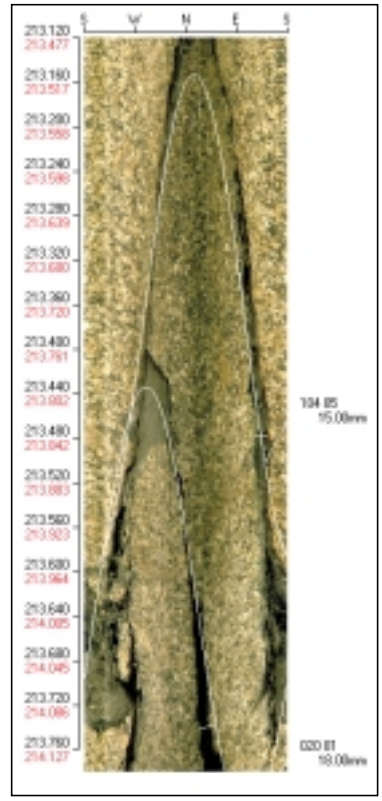

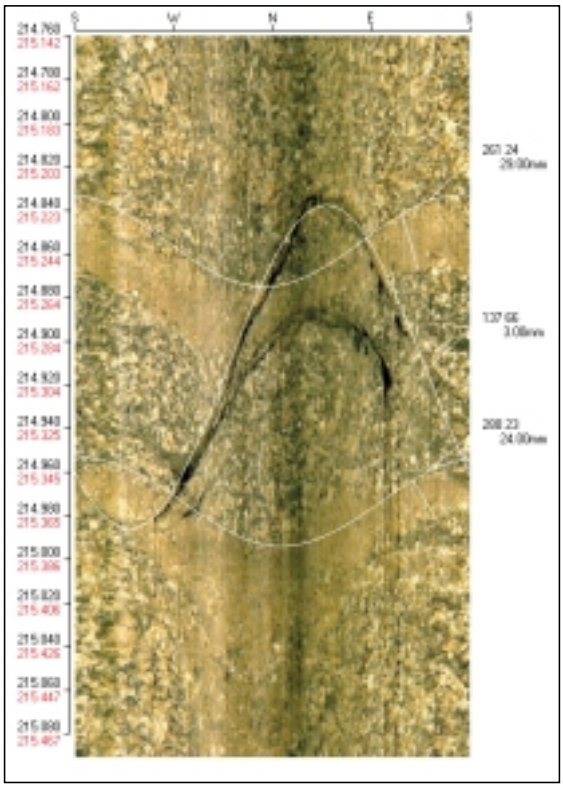

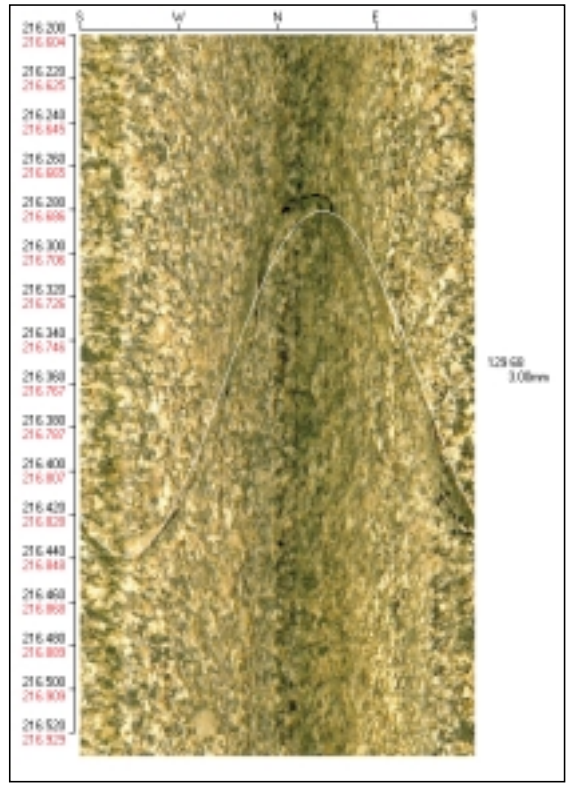

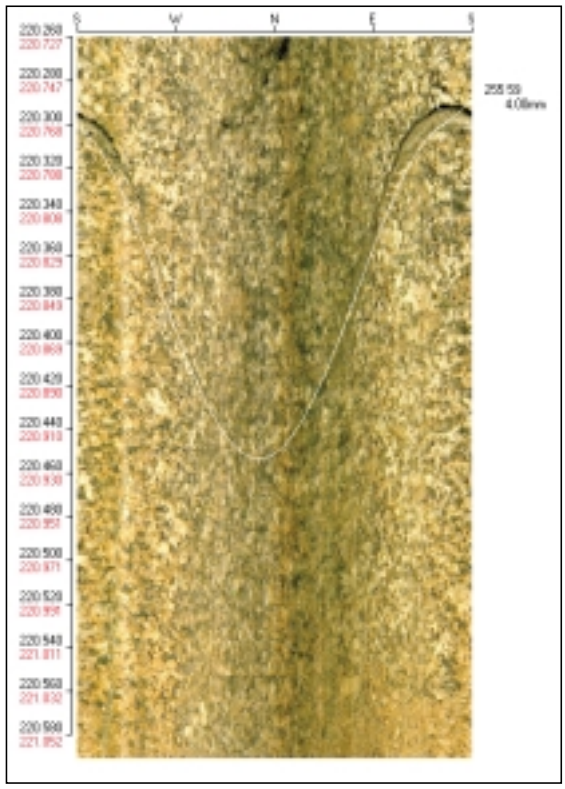

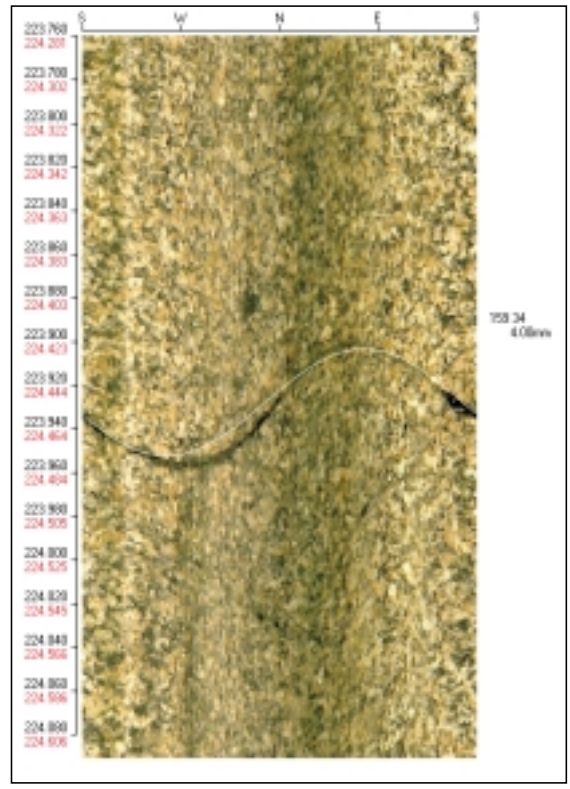

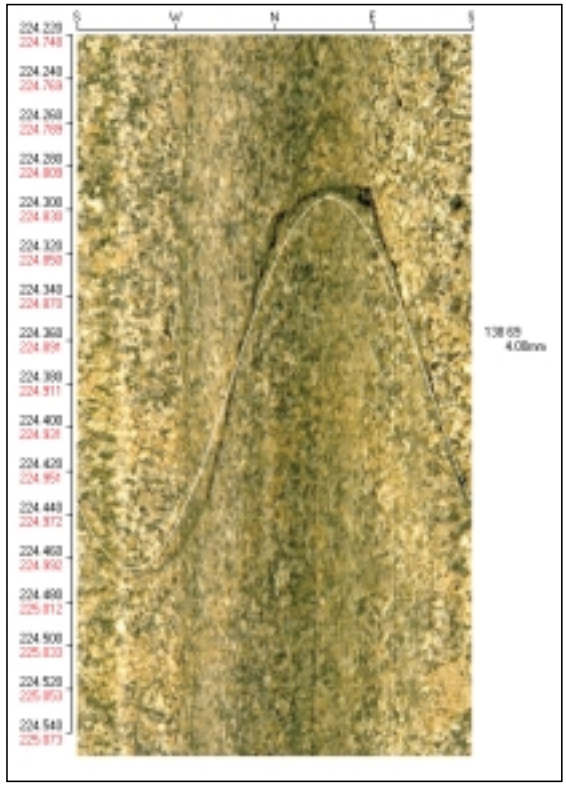

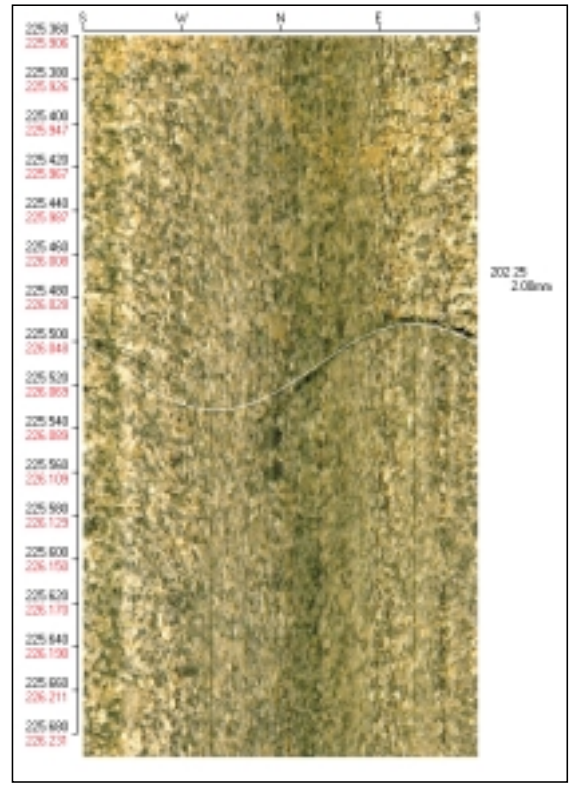

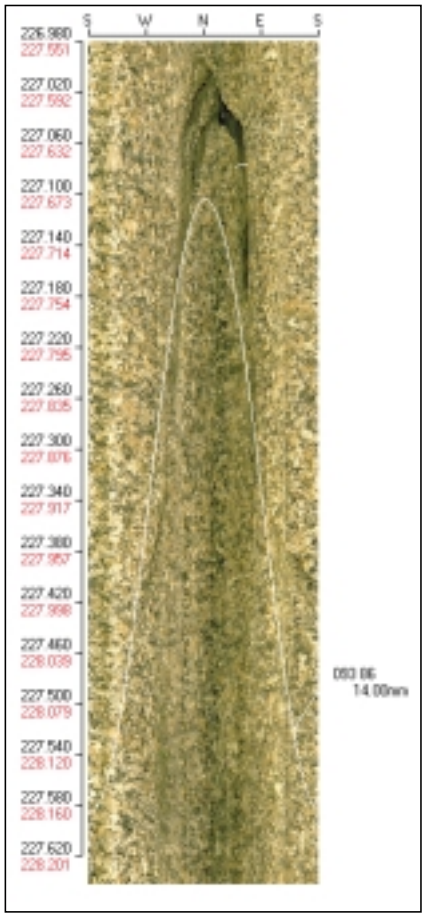
S W N E S
226.980
227.551
227.020
227.592
227.060
227.632
227.100
227.673
227.140
227.714
227.180
227.754
227.220
227.795
227.260
227.835
227.300
227.876
227.340
227.917
227.380
227.957
227.420
227.998
227.460
228.039
227.500
228.079
227.540
228.120
227.580
228.160
227.620
228.201
093.06
14.00ms

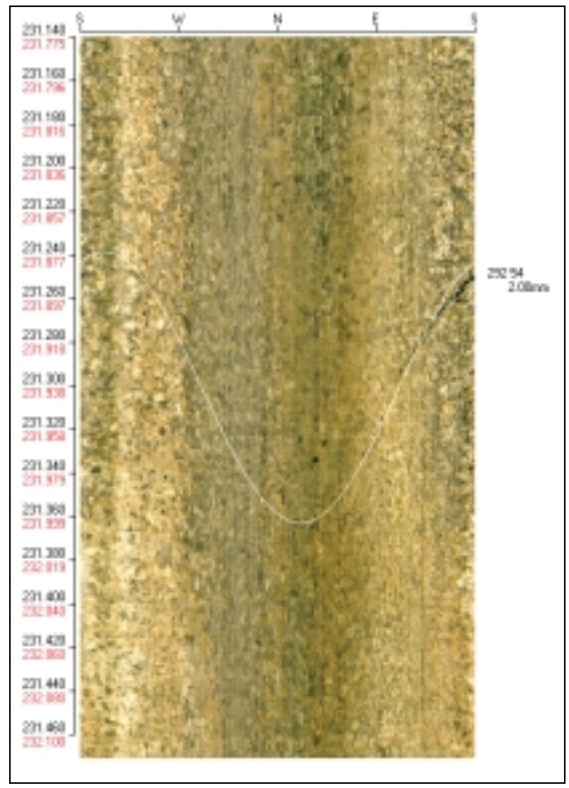
S W N E S
231.148
231.775
231.168
231.796
231.188
231.816
231.208
231.836
231.228
231.857
231.248
231.877
231.268
231.897
231.288
231.918
231.308
231.938
231.328
231.958
231.348
231.979
231.368
231.999
231.388
232.019
231.408
232.040
231.428
232.060
231.448
232.080
231.468
232.100
252.54
2.08ms

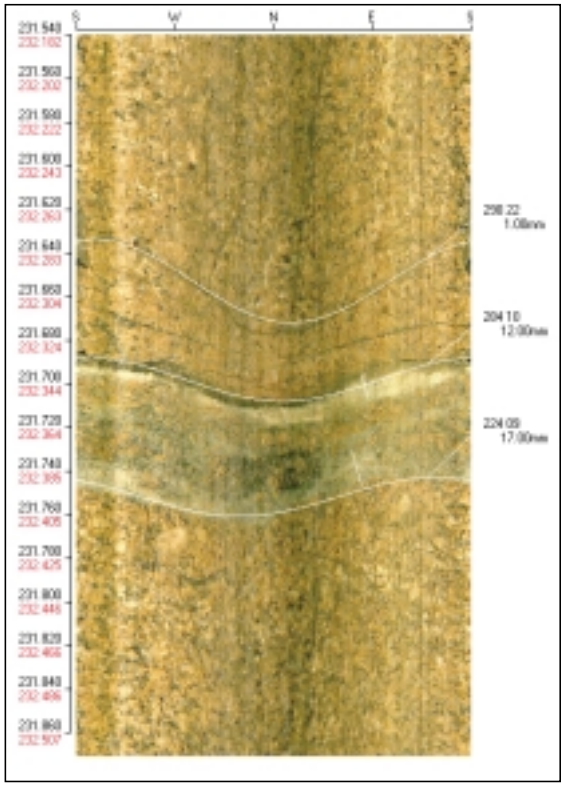
S W N E S
231.548
232.182
231.568
232.202
231.588
232.222
231.608
232.243
231.628
232.263
231.648
232.283
231.668
232.304
231.688
232.324
231.708
232.344
231.728
232.364
231.748
232.385
231.768
232.405
231.788
232.425
231.808
232.446
231.828
232.466
231.848
232.486
231.868
232.507
298.22
1.08ms
304.10
12.00ms
324.09
17.00ms

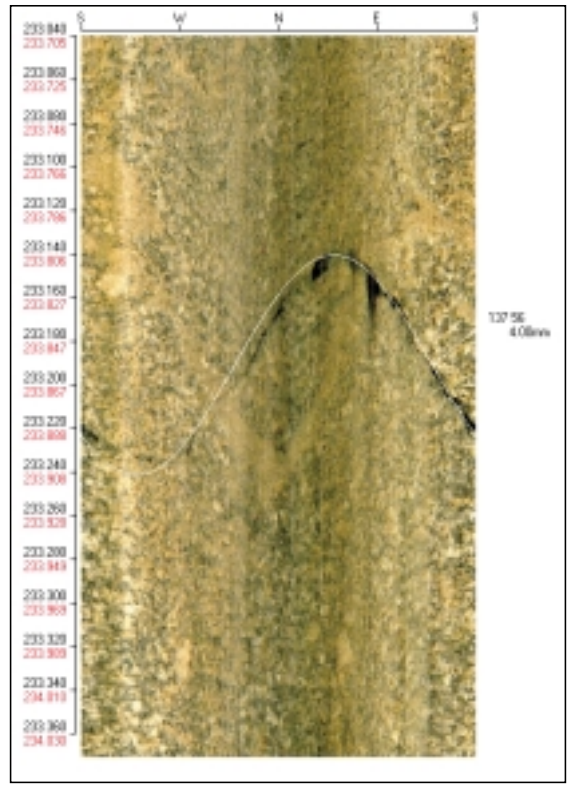
S W N E S
233.848
233.705
233.868
233.725
233.888
233.746
233.908
233.766
233.928
233.786
233.948
233.806
233.968
233.827
233.988
233.847
234.008
233.867
234.028
233.888
234.048
233.908
234.068
233.928
234.088
233.949
234.108
233.969
234.128
233.989
234.148
234.010
234.168
234.030
127.56
4.08ms

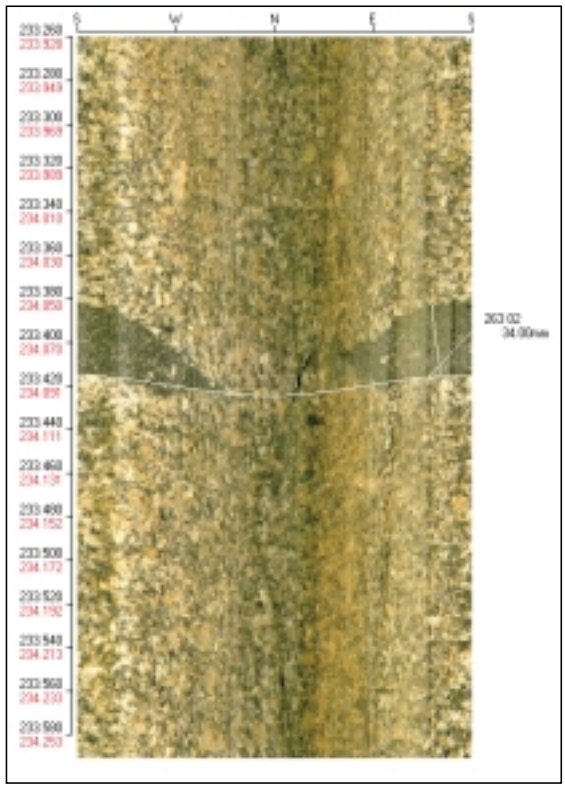

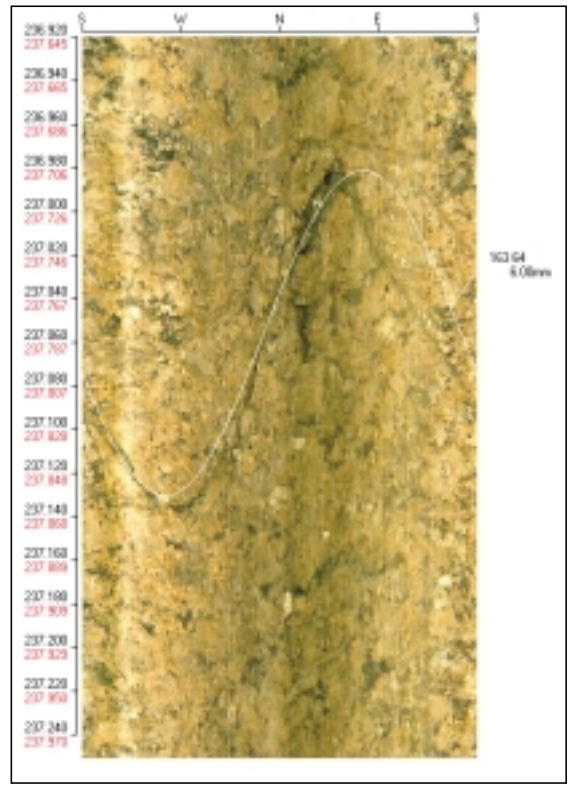

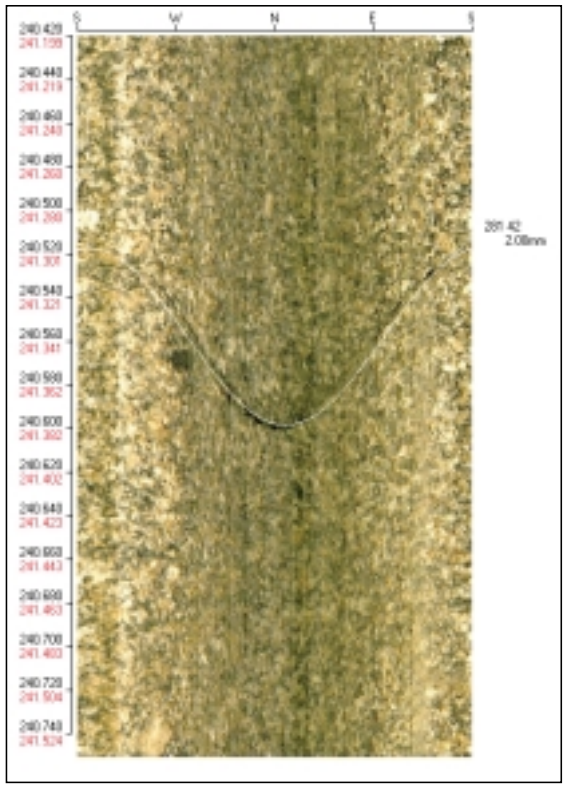

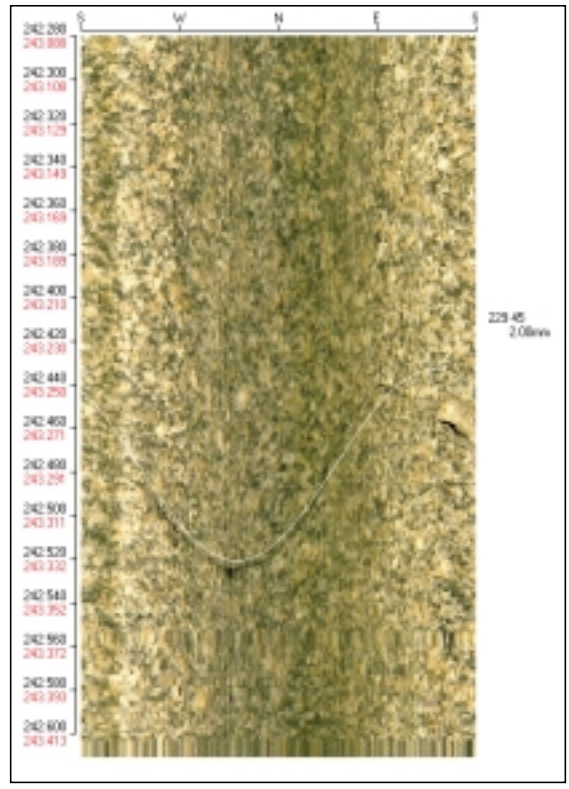

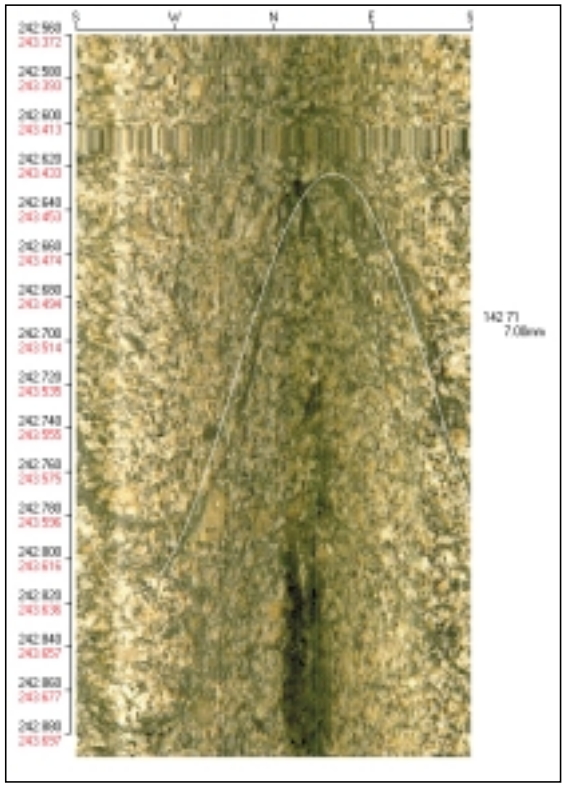
S W N E S
142.71
7.08ms

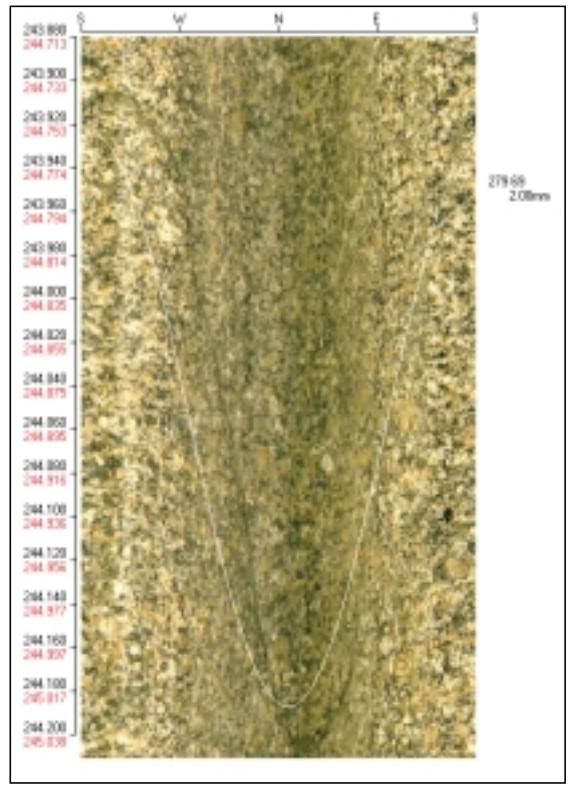
S W N E S
279.69
2.08ms

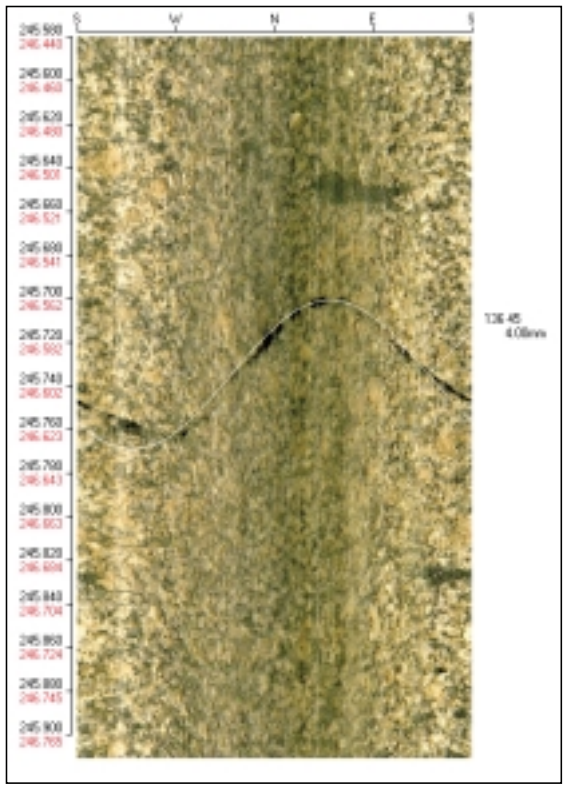
S W N E S
136.45
4.08ms

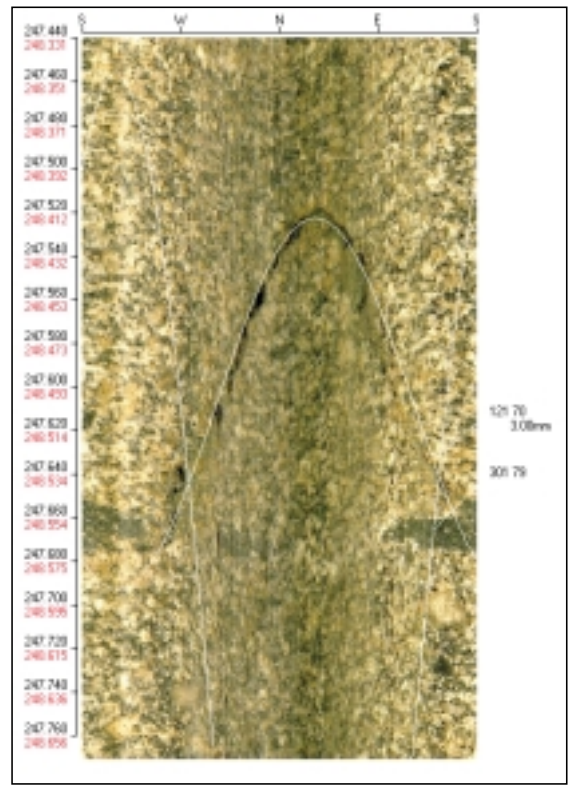
S W N E S
121.70
3.08ms
301.79

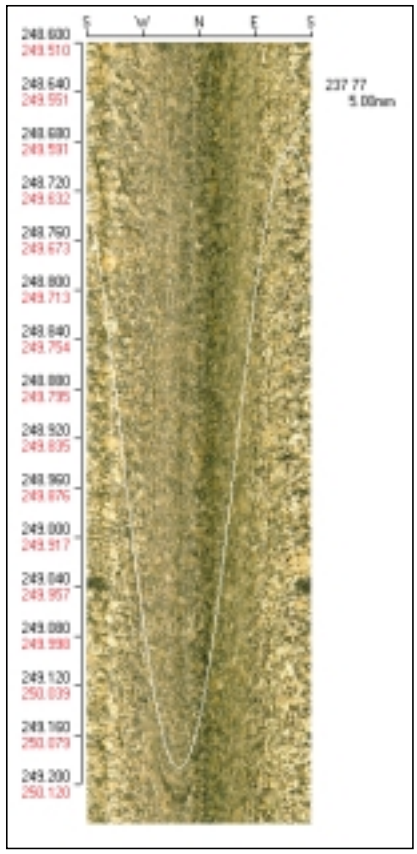
S W N E S
237.77
5.00mm

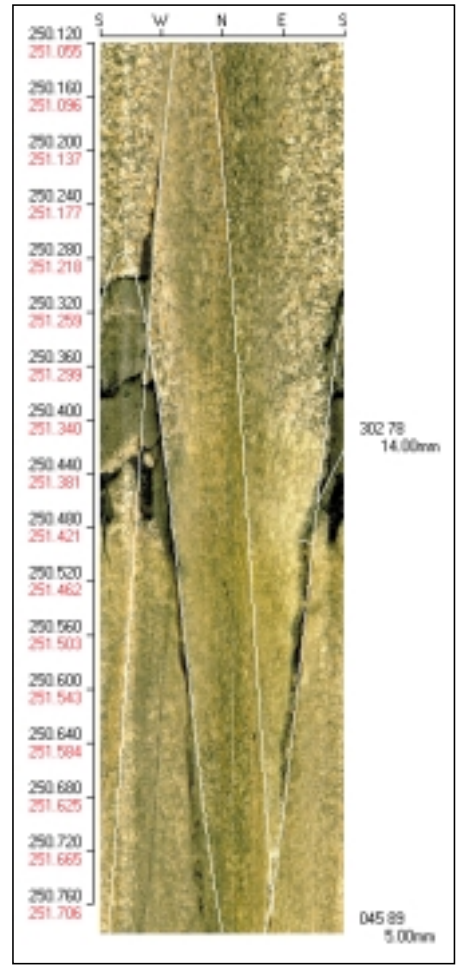
S W N E S
302.78
14.00mm
045.89
5.00mm

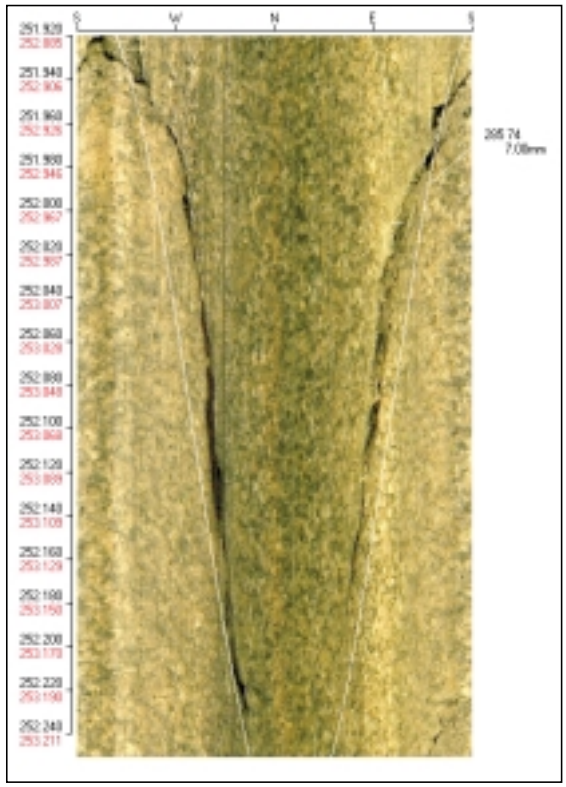
S W N E S
265.74
7.08mm

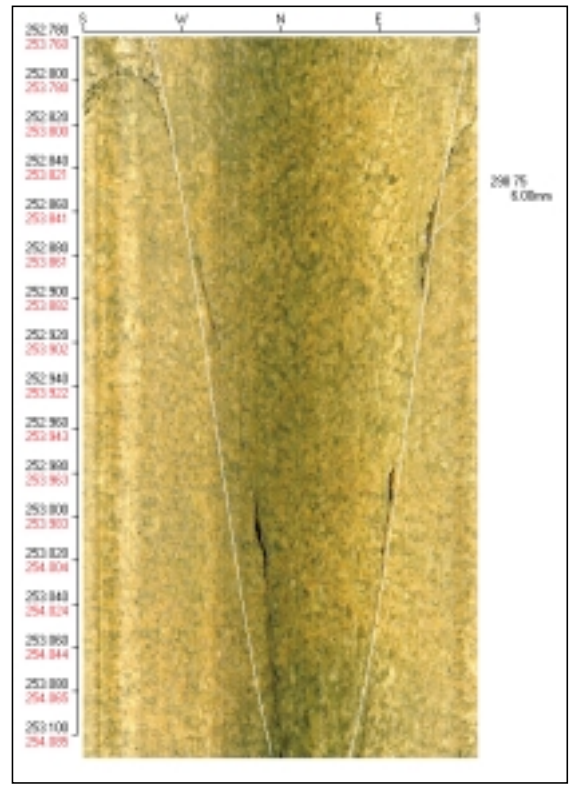
S W N E S
298.75
5.08mm

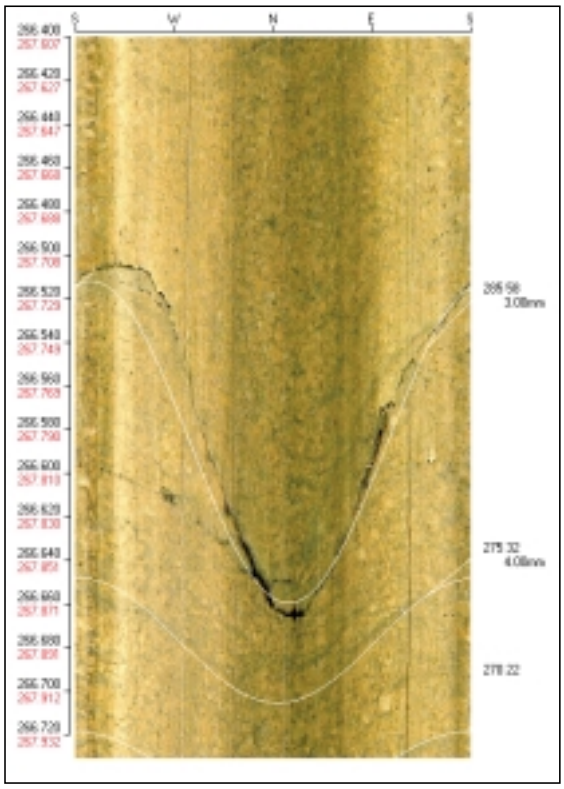
S
W
N
E
S
265.58
3.08mm
275.32
4.08mm
278.22

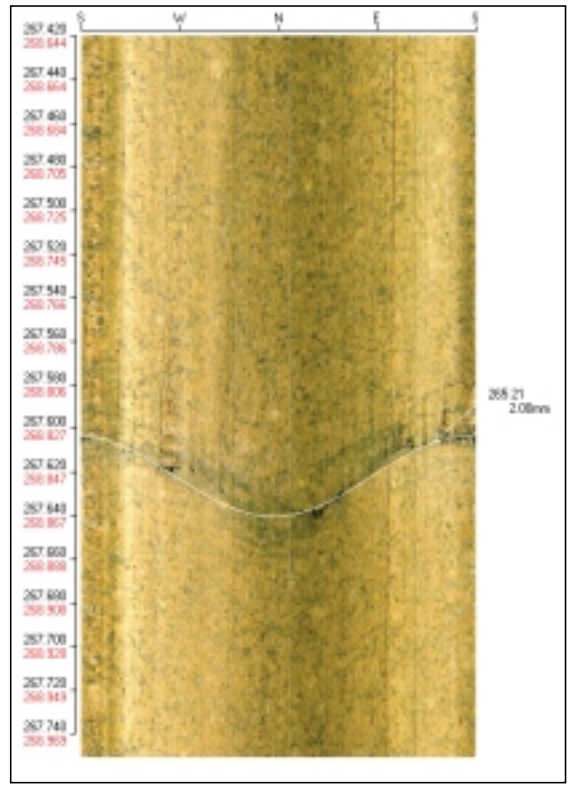
S
W
N
E
S
265.21
2.08mm

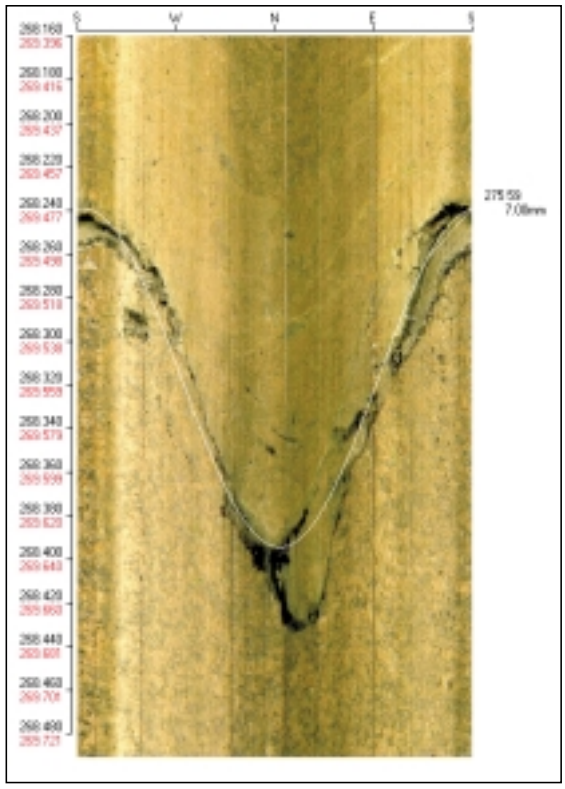
S
W
N
E
S
275.59
7.08mm

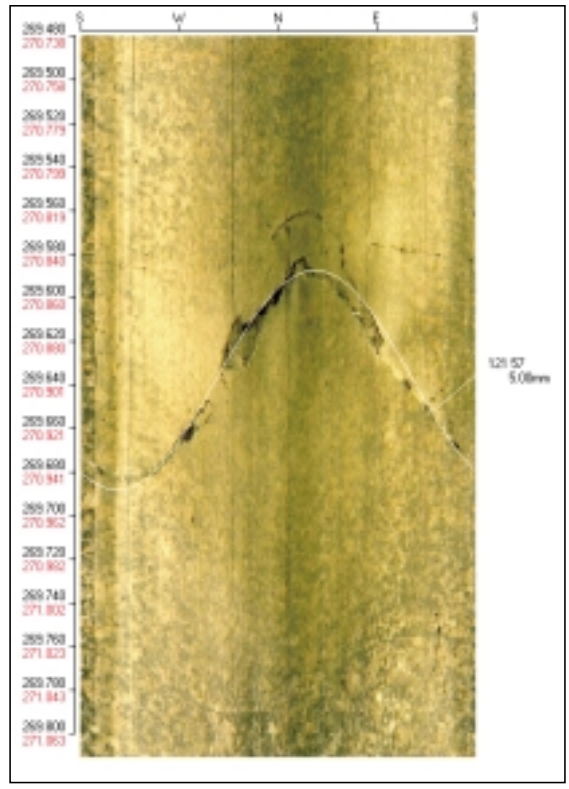
S
W
N
E
S
121.57
5.08mm

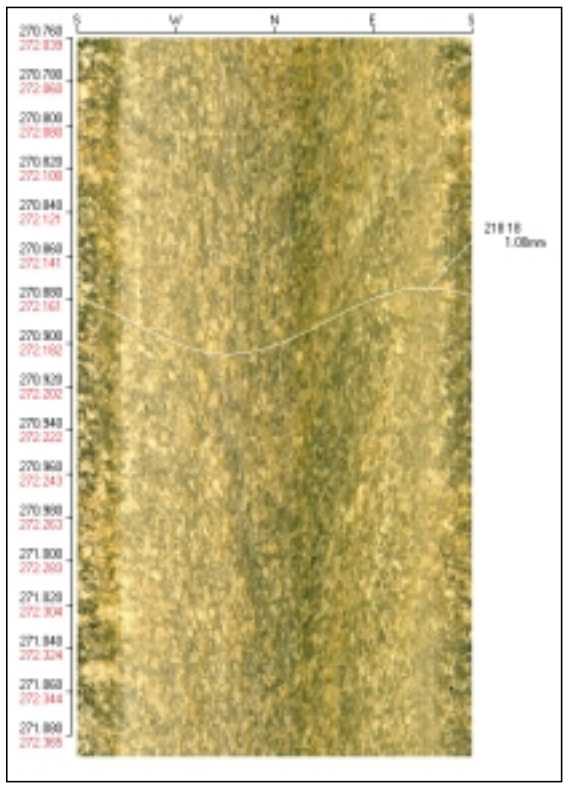

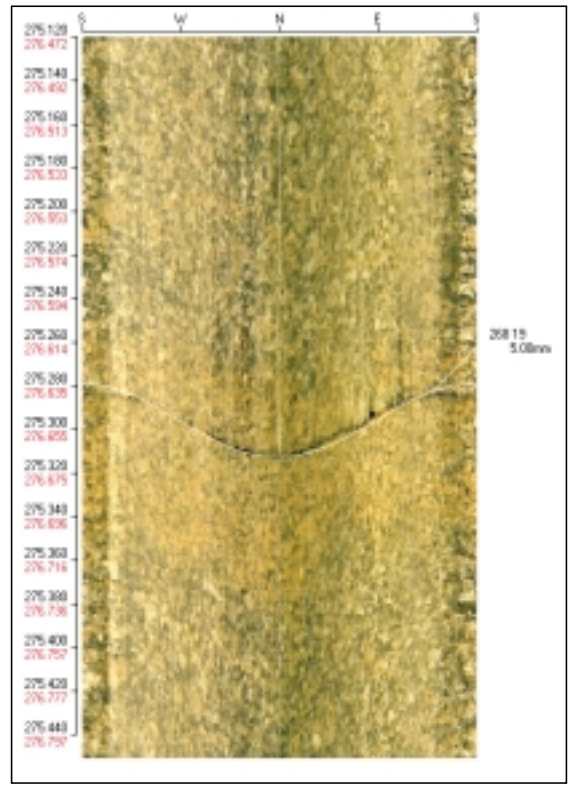

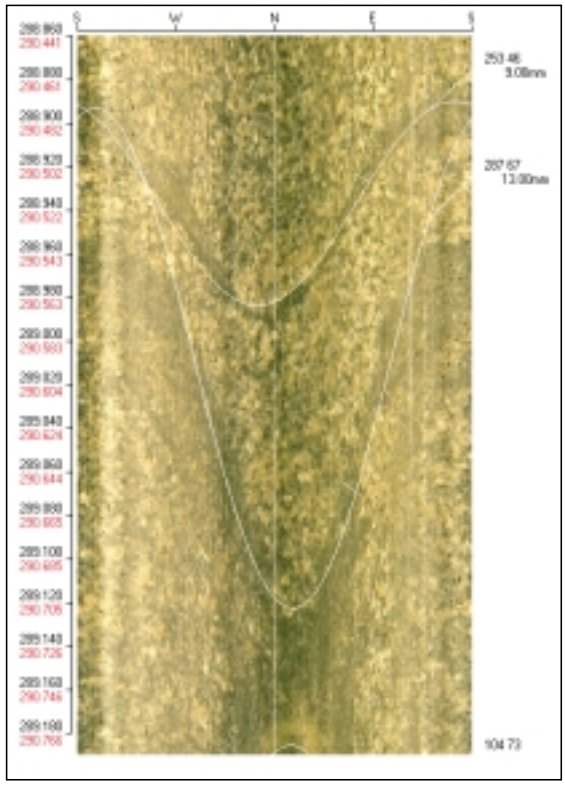

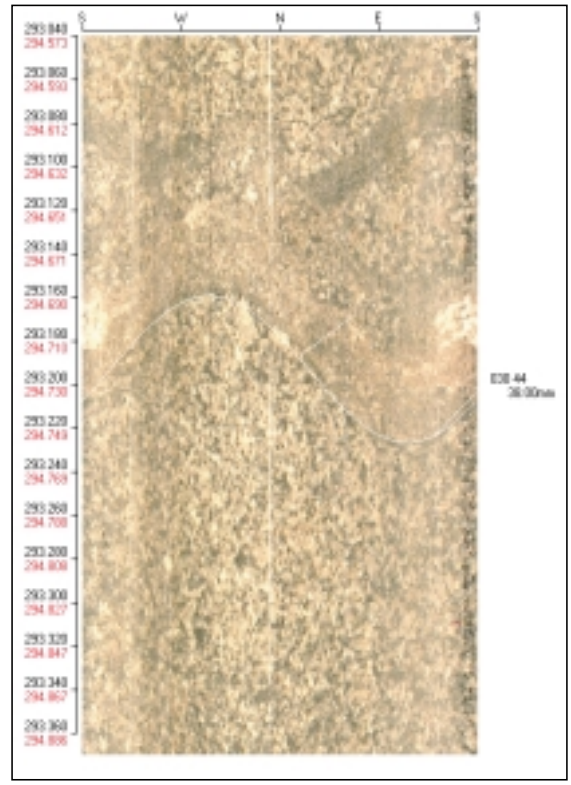

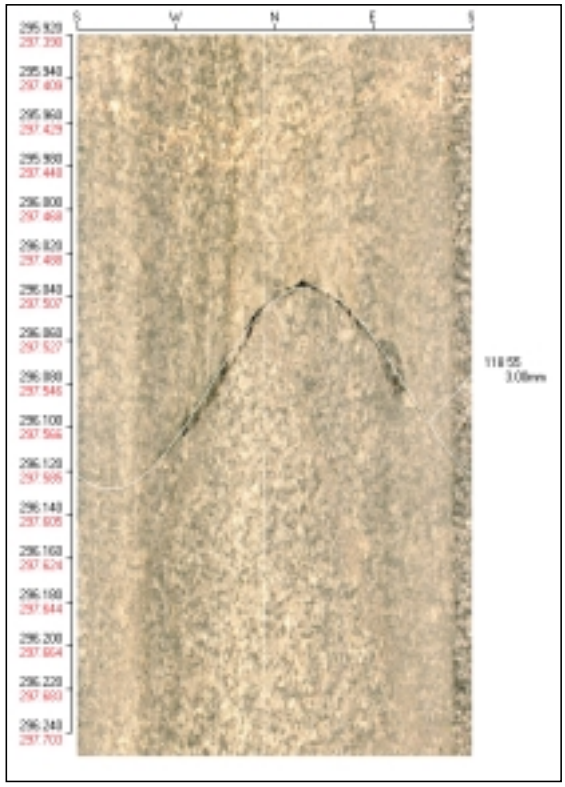
S
W
N
E
S
118.55
3.08mm

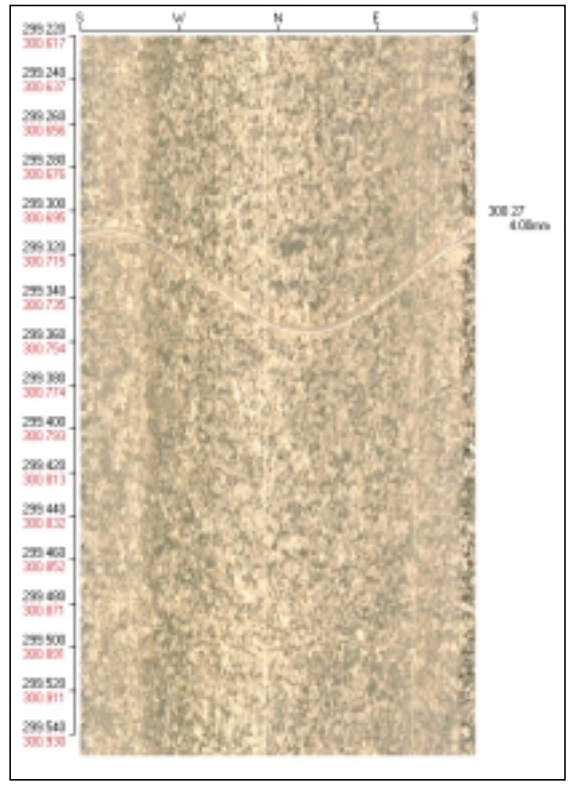
S
W
N
E
S
308.27
4.08mm

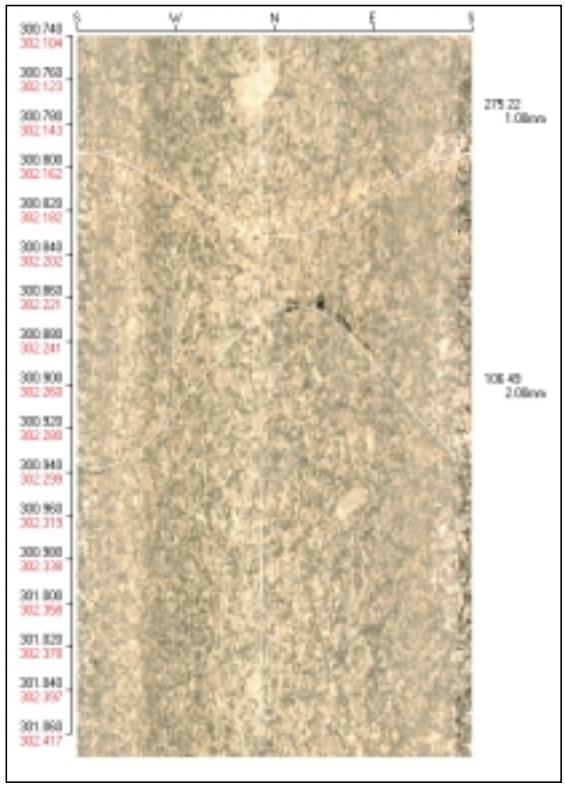
S
W
N
E
S
275.22
1.08mm
108.45
2.08mm

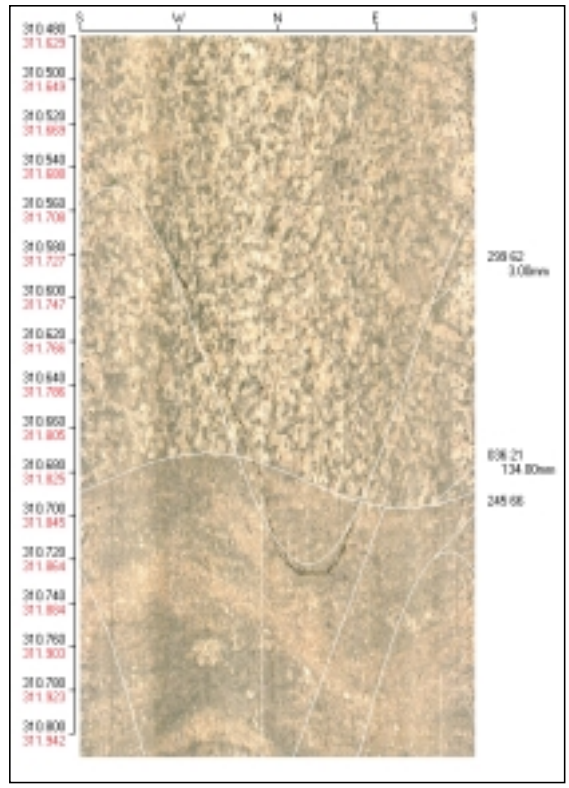
S
W
N
E
S
298.62
3.08mm
836.21
134.80mm
245.68

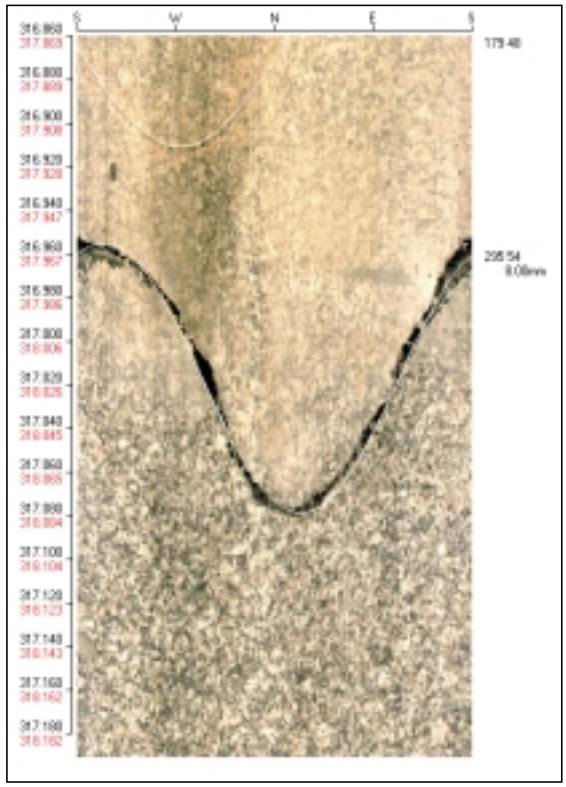

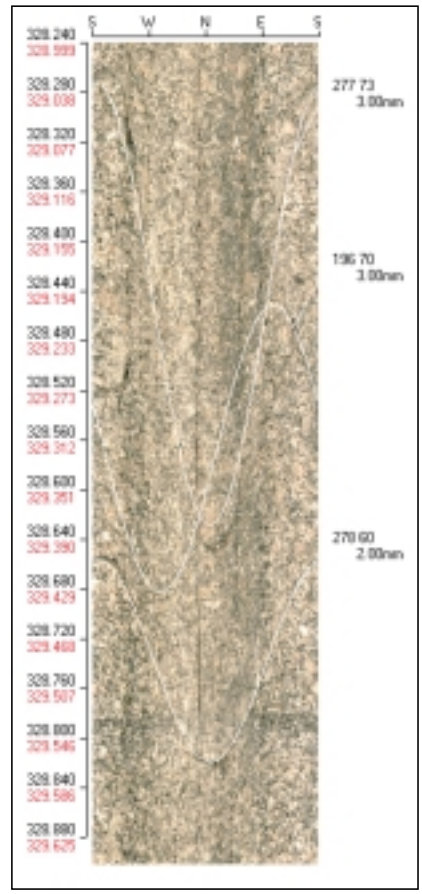

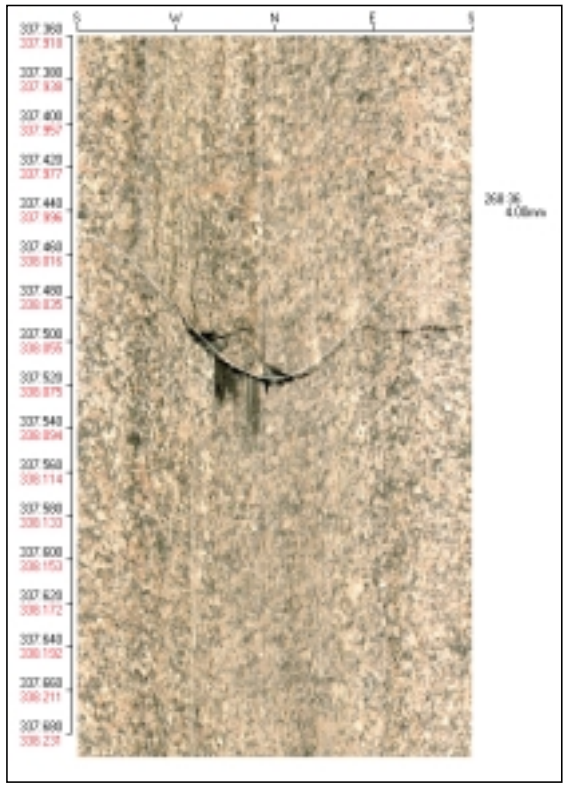

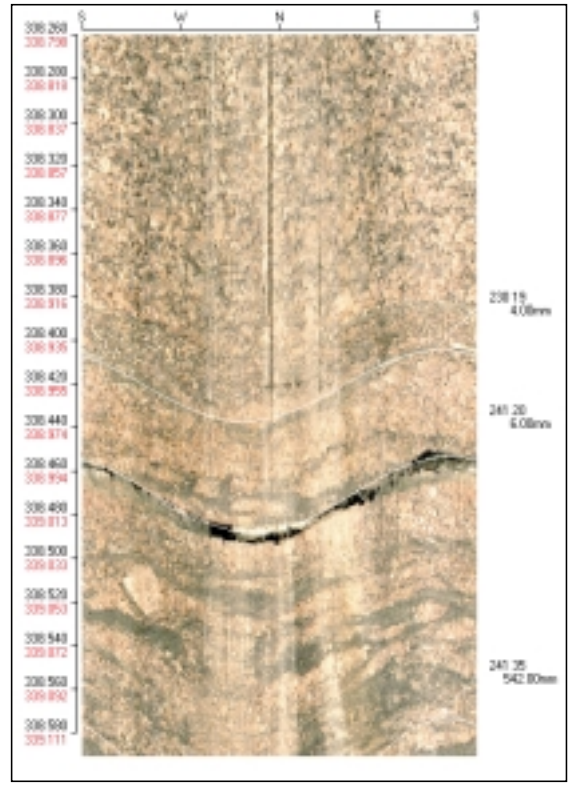

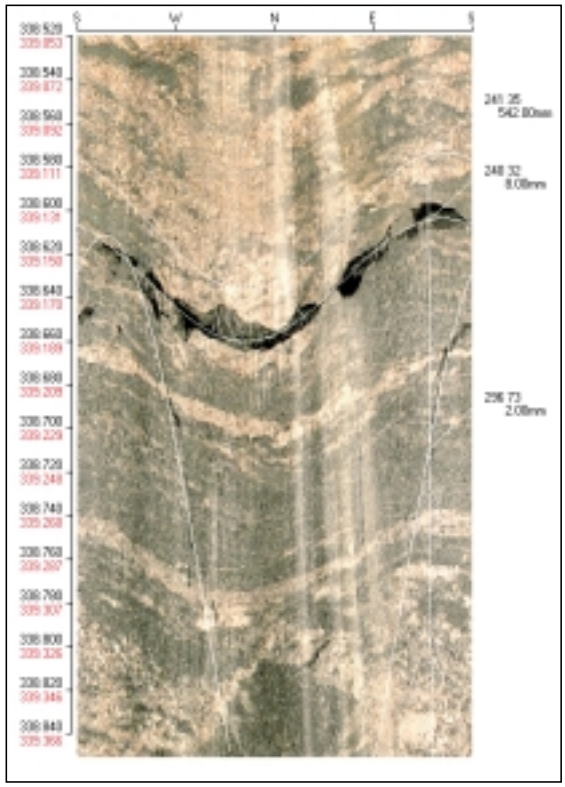

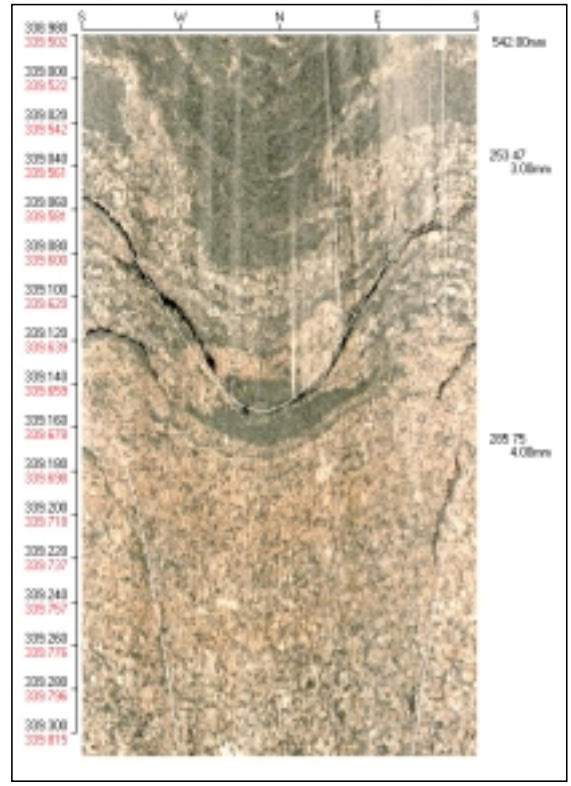

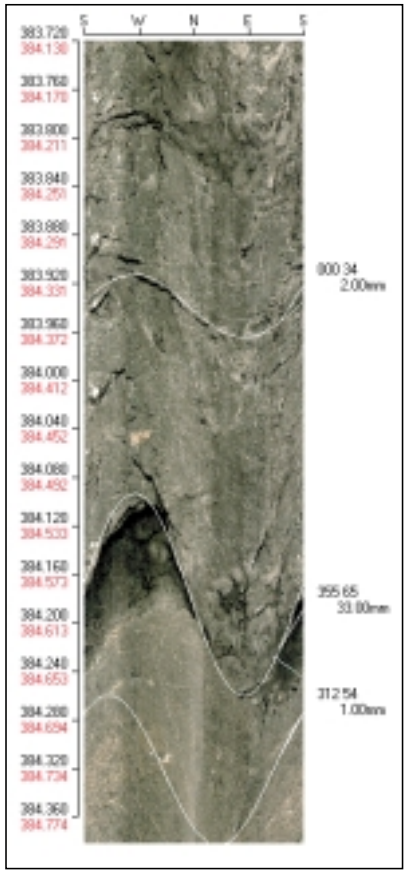

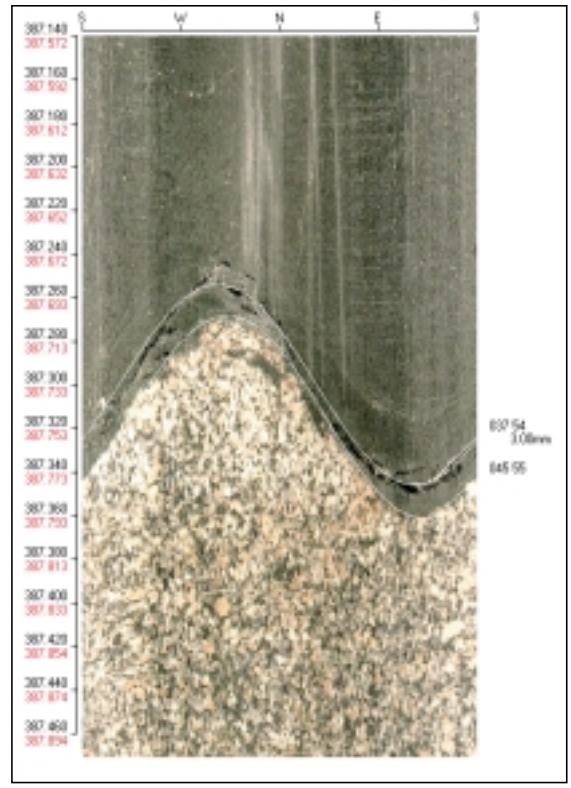

Appendix 5

Borehole radar images

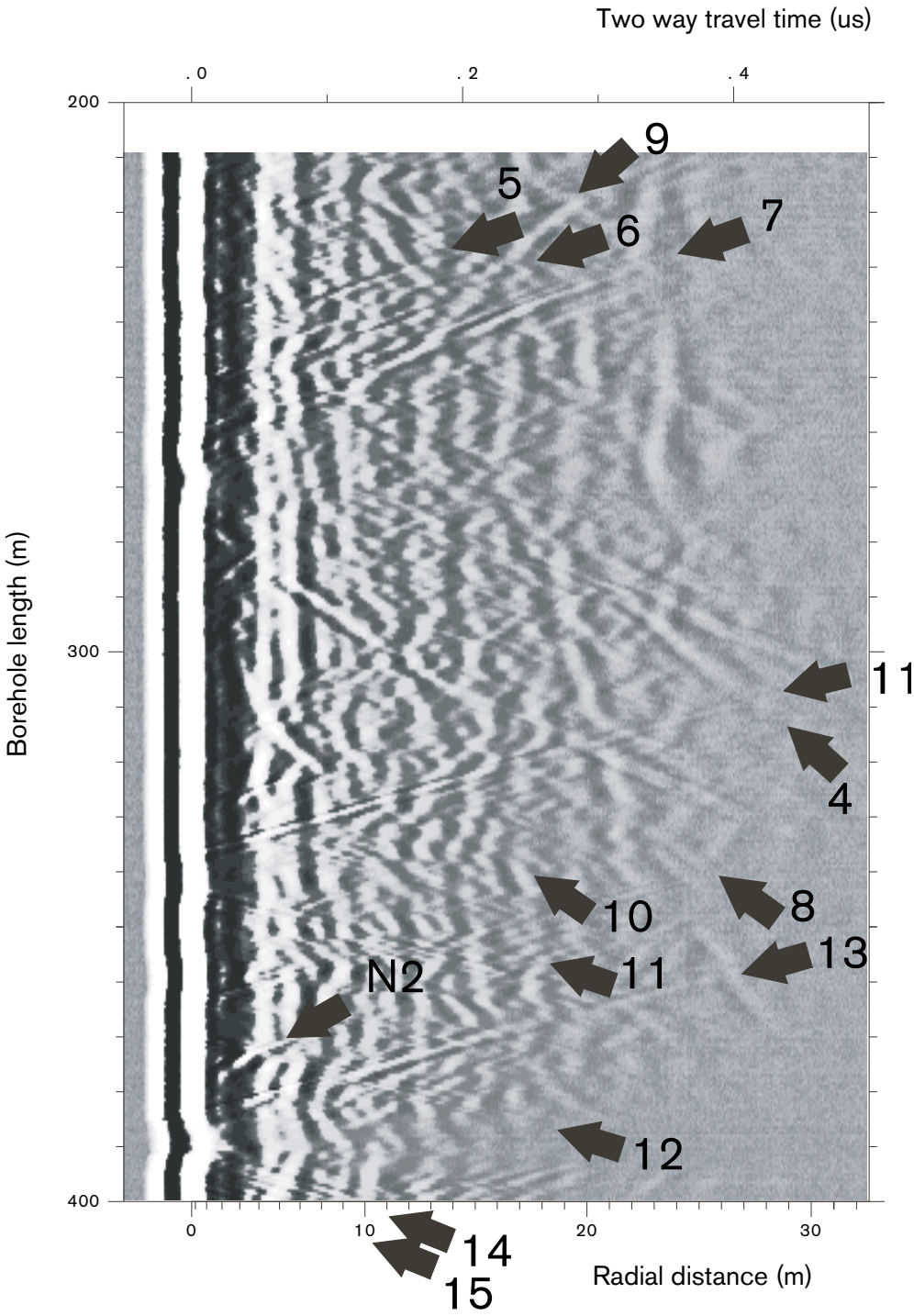
Two way travel time (us)
. 0
. 2
. 4
200
300
400
Borehole length (m)
0
10
20
30
Radial distance (m)
9
5
6
7
11
4
10
8
13
N2
11
12
14
15

Appendix 6

Correlation table between Borehole radar, BIPS and flow logging

Correlation of radar reflectors with BIPS and flow logging

Flow spot Length (m)	BIPS Length, adjusted (m)	BIPS Alpha (deg)	BIPS Orientation Strike/dip	BIPS Geological character	Bh-Radar Reflector (No. – Strength) 1=weak 2=medium 3=strong	Bh-Radar Length (m)	Bh-Radar Alpha (deg)	Bh-Radar Orientation Strike/dip	Bh-Radar Persistence (m)	Bh-Radar Correlation factor 3=Certain 2=Intermediate 1=Uncertain
212.0 213.3	212.1 213.7 (214.0)	17 9 (10)	119/77 104/85 (020/81)	Fracture Fracture open Fracture open	4–1	212	16	352/73	30	2
246.7	246.6	49	136/45	Fracture open	5–2	251	38	175/53	20	2
– –	260.3 (263.4)	55 (67)	321/32 (327/21)	Fracture oxidized Fracture oxidized	6–2	262	34	292/49	18	1
268.0	267.8	28	285/58	Fracture open	7–3	269	35	292/48	22	2
269.7	269.5	27	275/59	Fracture open	8–3	271	23	238/61	30	3
–	–				9–1	280	19	301/65	20	–
–	–				10–2	296	19	002/72	17	–
339.1	338.8	54	241/35	Fracture open	11–3	341	59	270/24	31+22	3
–	363.9	72	288/12	Vein chlorite	12–1	367	59	295/24	18	2
385.0	384.66	25	355/65	Fracture cavities and greenstone	N2–1	382	29	353/60 166/62	10+15	3
–	385.0 (385.3)	64 (62)	020/28 (347/27)	Fracture cavities and greenstone Vein calcite and greenstone	13–2	388	61	012/30	35	–
–	391.5	46	054/49	Vein pegmatite and greenstone	14–2	394	57	047/38	15	2
–	396.1	53	031/40	Vein pegmatite	15–1	396	44	045/51	15	3

Appendix 7

Combined correlation table

Combined correlation of DIFF flow, BIPS and Borehole radar

Classification of correlation: 1=Uncertain, 2=Medium, 3=Certain

Flow ml/h	Flowspot (m)	BIPS adjusted length (m)	BIPS Strike	BIPS Dip	Sort	Width (mm)	Conditions	BIPS Class	Bh-Radar length (m)	Bh-Radar strike	Bh-Radar dip	Bh-Radar persistence (m)	Bh-Radar Class
2964	212.0	212.121	119	77	Fracture	4	Cavities	3	212	352	73	30	2
158662	213.3	213.726	104	85	Fracture	15	Open	3	212	352	73	30	2
16757	214.0	213.987	20	81	Fracture	18	Open	1					
5031	215.2	215.289	137	66	Fracture	3	Cavities	3					
302	216.7	216.760	129	68	Fracture	3	Cavities	3					
572	220.7	220.839	255	59	Fracture	4	Cavities	3					
12542	224.4	224.447	159	34	Fracture	4	Open	3					
1823	224.9	224.907	138	69	Fracture	4	Cavities	3					
6625	226.0	226.056	202	25	Fracture	2	Cavities	3					
30680	227.7	227.918	93	86	Fracture	14	Oxidized	3					
778	231.9	231.937	292	54	Fracture	2	Dull	2					
38	232.4	232.395	224	9	Fracture	17	Oxidized	3					
5337	233.9	233.857	137	56	Fracture	4	Cavities	3					
166	234.2	234.090	263	2	Vein	34	Dull	3					
359	237.8	237.783	163	64	Fracture	6	Cavities	3					
86	238.0	238.073	174	53	Fracture	1	Cavities	3					
990	241.4	241.341	281	42	Fracture	2	Cavities	3					
121	242.3	242.573	125	26	Vein	5	Oxidized	1					
2870	243.3	243.290	229	45	Fracture	2	Cavities	2					
714	243.8	243.536	142	71	Fracture	7	Cavities	2					
733	244.9	244.894	279	69	Fracture	2	Dull	2					
22150	246.7	246.600	136	45	Fracture	4	Open	3	262	292	49	18	2
15479	248.6	248.502	121	70	Fracture	3	Cavities	3					
1623	249.2	249.277	213	70	Fracture	5	Dull	3					
578	250.1	249.851	237	77	Fracture	5	Cavities	1					
458764	251.3	251.476	45	89	Fracture	5	Oxidized	3					
111455	251.6	251.490	302	78	Fracture	14	Open	3					
41867	252.9	253.064	285	74	Fracture	7	Open	3					
1269	254.1	253.926	298	75	Fracture	6	Cavities	3					
16905	268.0	267.781	285	58	Fracture	3	Open	2	269	292	48	22	2
213	269.0	268.833	265	21	Fracture	2	Cavities	3					

Continued

Flow ml/h	Flowspot (m)	BIPS adjusted length (m)	BIPS Strike	BIPS Dip	Sort	Width (mm)	Conditions	BIPS Class	Bh-Radar length (m)	Bh-Radar strike	Bh-Radar dip	Bh-Radar persistence (m)	Bh-Radar Class
7977	269.7	269.539	275	59	Fracture	7	Open	3	271	238	61	30	3
36168	271.1	270.881	121	57	Fracture	5	Open	3					
715	273.8	272.153	218	18	Fracture	1	Dull	1					
0	275.0	274.271	146	54	Vein	16	Oxidized	1					
462	276.9	276.629	268	19	Fracture	5	Open	1					
796	290.5	290.558	287	67	Fracture	13	Dull	3					
219	292.6	294.699	30	44	Vein	38	Dull	1					
30324	295.1	296.966	110	41	Fracture	3	Cavities	3					
4393	295.6	297.505	118	55	Fracture	3	Cavities	3					
698	298.3	300.662	300	27	Fracture	4	Dull	1					
801	300.6	302.184	106	49	Fracture	2	Cavities	3					
0	307.9	309.379	307	16	Vein	8	Oxidized	3					
0	310.5	311.637	299	62	Fracture	3	Cavities	3					
0	314.7	315.589	301	65	Fracture	1	Cavities	2					
452519	317.1	317.833	295	54	Fracture	8	Open	1					
0	325.4	326.070	25	76	Fracture	2	Dull	3					
0	327.8	327.905	21	20	Fracture	3	Cavities	1					
0	328.6	328.936	277	73	Fracture	3	Cavities	3					
0	329.2	329.534	335	11	Vein	15	Dull	3					
0	332.7	332.570	281	38	Vein	10	Dull	1					
9576	337.9	337.707	268	36	Fracture	4	Cavities	1					
12983	338.9	338.665	241	20	Fracture	6	Open	3					
34185	339.1	338.822	240	32	Fracture	8	Open	3					
717	339.6	339.280	253	47	Fracture	3	Open	3					
0	377.2	377.319	283	36	Vein	5	Dull	2					
0	383.5	383.559	45	39	Contact	0	Dull	3					
c. 15000?	385.0	384.658	355	65	Fracture	33	Open	3	382	353	60	10+15	3
375	389.3	387.805	37	54	Fracture	3	Open	1					